

INFORMATION TO USERS

This manuscript has been reproduced from the microfilm master. UMI films the text directly from the original or copy submitted. Thus, some thesis and dissertation copies are in typewriter face, while others may be from any type of computer printer.

The quality of this reproduction is dependent upon the quality of the copy submitted. Broken or indistinct print, colored or poor quality illustrations and photographs, print bleedthrough, substandard margins, and improper alignment can adversely affect reproduction.

In the unlikely event that the author did not send UMI a complete manuscript and there are missing pages, these will be noted. Also, if unauthorized copyright material had to be removed, a note will indicate the deletion.

Oversize materials (e.g., maps, drawings, charts) are reproduced by sectioning the original, beginning at the upper left-hand corner and continuing from left to right in equal sections with small overlaps. Each original is also photographed in one exposure and is included in reduced form at the back of the book.

Photographs included in the original manuscript have been reproduced xerographically in this copy. Higher quality 6" x 9" black and white photographic prints are available for any photographs or illustrations appearing in this copy for an additional charge. Contact UMI directly to order.

UMI

A Bell & Howell Information Company
300 North Zeeb Road, Ann Arbor MI 48106-1346 USA
313/761-4700 800/521-0600



Determining Properties of
Neutralino Dark Matter
Using High-Energy Neutrino Events

Stefan H. P. Elieff

Department of Astronomy and Physics

Saint Mary's University

Halifax, Nova Scotia

Submitted in partial fulfillment of the
requirements for the degree of
Master of Science in Astronomy

June 1998

©1998 Stefan H. P. Elieff



**National Library
of Canada**

**Acquisitions and
Bibliographic Services**

395 Wellington Street
Ottawa ON K1A 0N4
Canada

**Bibliothèque nationale
du Canada**

**Acquisitions et
services bibliographiques**

395, rue Wellington
Ottawa ON K1A 0N4
Canada

Your file Votre référence

Our file Notre référence

The author has granted a non-exclusive licence allowing the National Library of Canada to reproduce, loan, distribute or sell copies of this thesis in microform, paper or electronic formats.

The author retains ownership of the copyright in this thesis. Neither the thesis nor substantial extracts from it may be printed or otherwise reproduced without the author's permission.

L'auteur a accordé une licence non exclusive permettant à la Bibliothèque nationale du Canada de reproduire, prêter, distribuer ou vendre des copies de cette thèse sous la forme de microfiche/film, de reproduction sur papier ou sur format électronique.

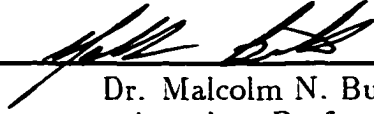
L'auteur conserve la propriété du droit d'auteur qui protège cette thèse. Ni la thèse ni des extraits substantiels de celle-ci ne doivent être imprimés ou autrement reproduits sans son autorisation.

0-612-33841-X

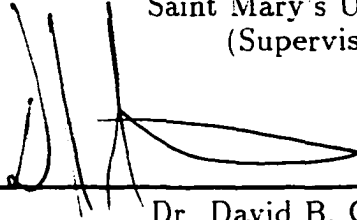
Canada

Certificate of Examination

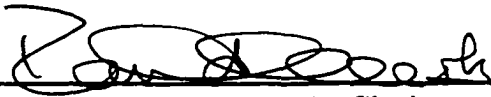
Saint Mary's University
Department of Astronomy and Physics



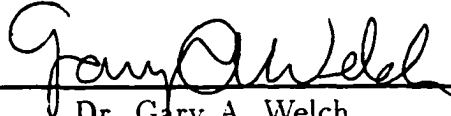
Dr. Malcolm N. Butler
Associate Professor
Department of Astronomy and Physics
Saint Mary's University
(Supervisor)



Dr. David B. Guenther
Associate Professor
Department of Astronomy and Physics
Saint Mary's University



Dr. David A. Clarke
Associate Professor
Department of Astronomy and Physics
Saint Mary's University



Dr. Gary A. Welch
Associate Professor
Department of Astronomy and Physics
Saint Mary's University



Dr. Glenn D. Starkman
Associate Professor
Department of Physics and of Astronomy
Case Western Reserve University
(External Reader)

Contents

Abstract	1
1 Introduction	2
1.1 Observational Evidence for Dark Matter	3
1.2 Theoretical Motivation for Dark Matter	6
2 Supersymmetry	9
2.1 The Standard Model of Particle Physics	9
2.2 Shortcomings of the Standard Model	11
2.3 Supersymmetric Particle Spectrum	12
2.4 Benefits of Supersymmetry	14
2.5 R -parity and the Neutralino	15
2.6 Relic Abundance	17
3 Indirect Detection of Neutralinos	21
3.1 Supersymmetric Models	23
3.2 Constraints	24
3.3 Capture in the Sun and Earth	28
3.4 $\chi\bar{\chi}$ Annihilation and Determining Event Rates	29
3.4.1 Charm and bottom quark decay	32
3.4.2 τ lepton decay	33
3.4.3 Top quark decay	34
3.4.4 W and Z boson decay	35
3.4.5 Higgs and Higgs-gauge boson decay	36
4 Determining Neutralino Properties	39
4.1 Direct Relationships	39

4.2	Sun-Earth Event Ratio	46
4.2.1	Neutralino Capture	46
4.2.2	Equilibrium Time Scale	51
4.3	Practical Application of the Neutralino Density Estimate	56
4.3.1	Neutralino Mass and Annihilation Cross Section Ratio	60
4.3.2	Relating Event, Capture, and Annihilation Rates	60
4.3.3	Scalar versus Axial-Vector Interactions	68
5	Discussion and Conclusion	69

List of Figures

1	Rotation curve for NGC6503	4
2	Number density of neutralinos in the early universe	19
3	M_2 - μ plane of parameter space	29
4	Event rate versus M_2	40
5	Event rate versus m_χ	41
6	Event rate versus $\Omega_\chi h^2$	44
7	Event rate versus f_g	45
8	Comparison of three solar event rates	47
9	$\Gamma_\ominus/\Gamma_\oplus$ versus m_χ	50
10	$\Gamma_\ominus/\Gamma_\oplus$ versus f_g	51
11	Estimated upper limit on $\Omega_\chi h^2$	55
12	Estimation of $\Omega_\chi h^2$	57
13	Earth event rate versus $\Gamma_{A\oplus} m_\chi^2$	58
14	Estimated lower limit on $\Omega_\chi h^2$	59
15	κ versus m_χ	61
16	Solar event rate versus $\Gamma_{A\odot} m_\chi^2$	63
17	Re-calculation of upper limit on $\Omega_\chi h^2$	64
18	Re-calculation of estimated $\Omega_\chi h^2$	65
19	Re-calculation of lower limit on $\Omega_\chi h^2$	66
20	Capture ratio γ for a range of m_χ	67

List of Tables

1	Standard model particles	10
2	Supersymmetric particles	13
3	Range of MSSM parameters explored.	24
4	Constraints used to eliminate SUSY models	25

Abstract

Determining Properties of Neutralino Dark Matter Using High-Energy Neutrino Events

Stefan H. P. Elieff

June 1998

Observational evidence and theoretical arguments indicate that most of the universe is made of dark matter. Supersymmetry, an extension of the standard model of particle interactions, provides a natural candidate for dark matter: a weakly interacting massive particle (WIMP) called the neutralino. The next generation of high-energy neutrino telescopes could detect these particles indirectly from the neutrinos created when they annihilate after being captured in the Sun and Earth. The possibility of determining neutralino properties based on these neutrino fluxes is investigated for a range of supersymmetric models. Of particular interest is the ratio of events from the Sun and Earth, a quantity that may provide information about neutralino mass and relic density in the universe.

1 Introduction

The hot big bang theory of the evolution of the universe is one of the successes of modern physics. It explains the expansion of the universe first observed in the 1920's, the large scale isotropy and homogeneity of the universe, and the existence of the cosmic microwave background radiation (CMBR). Through measurements of the expansion rate, the theory predicts an age for the universe consistent with other independent determinations [1]. Furthermore, standard big bang nucleosynthesis (SBBN) explains the observed primordial abundances of elements in the universe [2]. In particular, light elements such as deuterium and helium-4 are important because there are no other known astrophysical processes that can produce the observed abundances of these elements. Deuterium, for example, is so easily destroyed that even the small amount present in the universe is nearly impossible to explain without primordial nucleosynthesis.

In reproducing observed light element abundances, SBBN places strong constraints on the amount of baryonic matter that is present in the universe. The mass density of baryons must lie in the range $0.01 \leq \Omega_b h^2 \leq 0.015$ [2]. Ω is the cosmological density parameter which is defined as ρ/ρ_c , where ρ_c is the critical density of the universe. The subscript b indicates the baryonic matter contribution $\Omega_b = \rho_b/\rho_c$. Uncertainty in the Hubble constant H_o affects the SBBN bound on Ω_b and is accounted for through the parameter h . Defining $H_o = 100 h \text{ km sec}^{-1} \text{ Mpc}^{-1}$, the broadest range of values for the Hubble constant consistent with current observations and analysis is $h = 0.4\text{--}1.0$. Including this uncertainty means $0.01 \leq \Omega_b \leq 0.1$. The total luminous mass density amounts only to $\Omega_{\text{lum}} < 0.01$ [3]. A wide range of observations consistently indicates there is more mass than luminous matter alone can explain. There must therefore be a significant amount of "dark matter" in the universe.

1.1 Observational Evidence for Dark Matter

Rotation curves of spiral galaxies are some of the most compelling evidence for the existence of dark matter. When the radial distance r becomes greater than the extent of the light, the velocity should drop $\propto r^{-\frac{1}{2}}$ (Keplerian orbits). Measurements made on neutral hydrogen clouds in spiral galaxies, using 21 cm emissions, show that the rotational velocities of the clouds remain constant as far from the galaxy centre as one can probe. Using Newton's law for circular motion,

$$\frac{GM(r)}{r^2} = \frac{v^2}{r}, \quad (1)$$

the constant rotational velocity means the galactic mass as a function of radius $M(r) \propto r$ out to large radii, implying there is mass well beyond the visible extent of the galaxy. A classic example of this is the rotation curve for NGC 6503 shown in Figure 1 [4]. The luminous disk of the galaxy extends only 5 kpc from the core, yet the rotation curve remains flat to at least 20 kpc. The analysis in [4] suggests this results from a dark halo. Flat, extended rotation curves are typical for spiral galaxies, including the Milky Way, and they imply the existence of large dark halos that surround spiral galaxies and contribute invisibly to their mass.

The presence of dark halos means the mass to light ratio M/L increases as you move further from the galactic centre. Through estimates of M/L , the amount of matter contained in the dark halo of spiral galaxies is inferred to be at least 2–10 times the upper luminous matter limit, $\Omega_{\text{lum}} < 0.01$ [3]. Another method for determining the mass of spiral galaxies is measuring the motion of the small gravitationally bound dwarf galaxies that surround them. This method produces a lower bound of $\Omega_{\text{spirals}} \gtrsim 0.087h^{-1}$, which is also well above the density of luminous matter [5]. Nearly all measurements of Ω are above the value that can be explained with only luminous matter. This makes up the primary evidence for dark matter.

Dark matter is not restricted to spiral galaxies; the velocity dispersion within

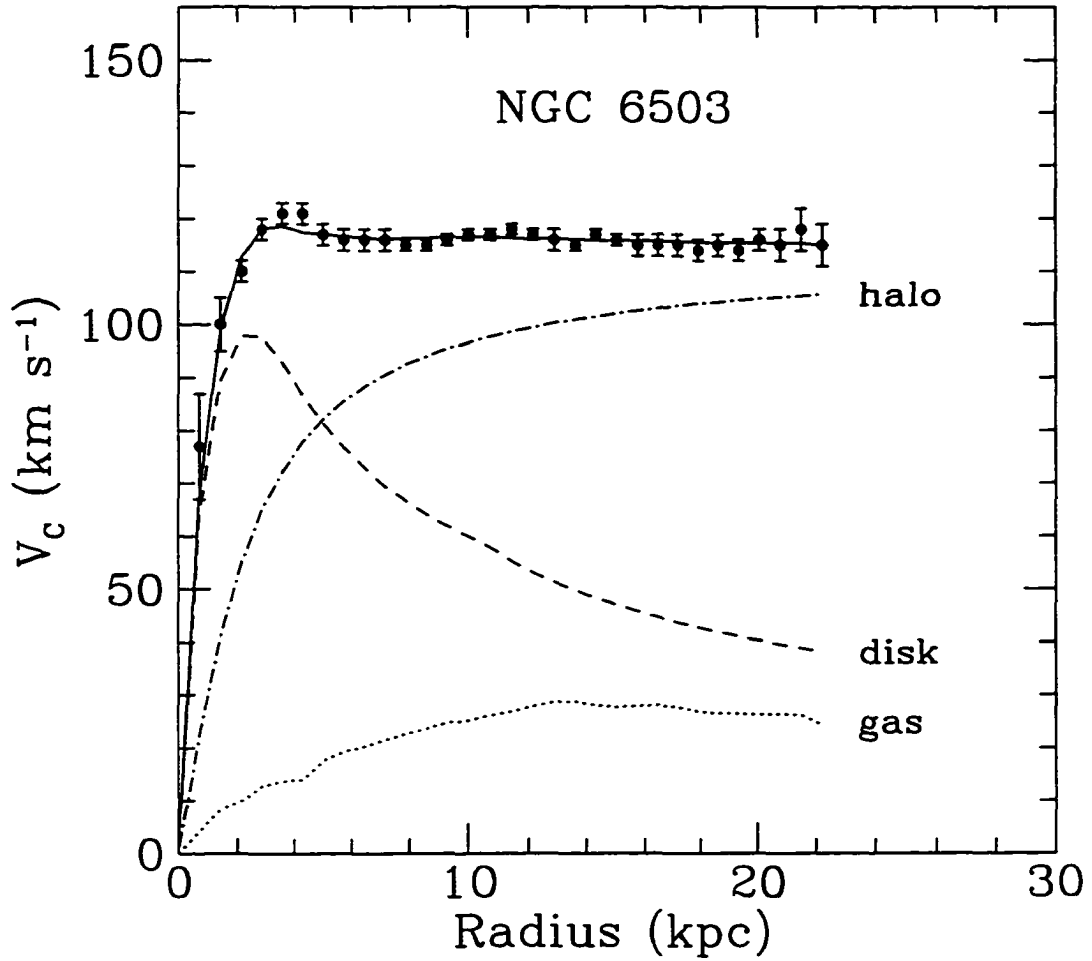


Figure 1: Rotation curve for the spiral galaxy NGC6503. The points are the measured circular rotation velocities as a function of distance from the centre of the galaxy. The dashed and dotted curves are the contribution to the rotational velocity due to the observed disk and gas, respectively, and the dot-dash curve is the inferred contribution from the dark halo. (From [4]).

elliptical galaxies also suggests the presence of dark matter [6]. In addition to this, elliptical galaxies can be studied using hot X ray emitting gas to find their mass distributions. X ray gas often extends well beyond the visible extent of the galaxy, implying high mass to light ratios and significant amounts of dark matter. Assuming hydrostatic equilibrium and using an isothermal model, Fabricant and Gorenstein [7] found that the mass of the gas was only 5% of the total mass of the elliptical galaxy M87 inferring a value of $\Omega_{\text{elliptical}} \sim 0.2$.

On larger scales, clusters of galaxies can be tested for the existence of dark matter. Several methods exist, such as X ray gas measurements similar to those described above, gravitational lensing, and using the velocity dispersion of cluster members to yield masses. Observations of the Coma cluster imply $\Omega = 0.2-0.4$ if the inner 1.5 Mpc is representative of the entire universe [8].

It is possible to determine values for Ω on still greater scales, although the uncertainties become larger with the increased model dependence of the methods. Even for clusters of galaxies, it is difficult to conclude whether the amount of dark matter detected is characteristic of the universe as a whole or is instead a local phenomenon. It is therefore important to measure dark matter at the largest scales. This is possible through measurements of large scale flows. The simplest example of this is the local group of galaxies' motion relative to the cosmic microwave background. If this motion is due to a gravitational excess, then the velocity should point towards an excess of mass. By using galaxy counts in the direction of motion and relating this to the excess mass, very conservative estimates of $\Omega > 0.2$ have been made [9]. It is also possible to estimate Ω from the distribution of peculiar velocities of galaxies. Comparisons of the peculiar velocity field to the galaxy density in the IRAS galaxy catalogue indicate that $\Omega > 0.33$, and the data is consistent with $\Omega = 1$ [10].

Gravitational lensing can be applied in the search for dark matter on large scales, in addition to measuring the masses of individual clusters of galaxies. This is ac-

completed by searching for microlensing events involving extremely distant objects, such as quasars, in much the same way as current searches for MACHOs (Massive Compact Halo Objects) in our galaxy are carried out. If there is a significant density ($\Omega \sim 1$) of compact bodies in the universe, distant objects will frequently be gravitationally lensed by these bodies. A long term study by Hawkins [11] measured light variations in quasars. Based on the number and nature of events in the study, Hawkins concluded a population of lenses with typical mass around $10^{-3}M_{\odot}$ exists. Estimates of Ω from the observations are weak, with a best fit cosmological density of $\Omega = 0.5$.

1.2 Theoretical Motivation for Dark Matter

There are theoretical arguments for the existence of dark matter. The standard theory of inflationary cosmology prefers $\Omega = 1$. If the universe has a non-zero vacuum energy density it can undergo a phase transition that leads to exponential growth, driving Ω to essentially 1 and producing the observed isotropic, homogenous universe [12]. Non-inflationary cosmology is unable explain an isotropic universe without invoking very special initial conditions [13]. In addition, a non-inflationary universe that has a value of $\Omega \neq 1$ will have its density rapidly driven away from the critical value as it evolves. For Ω to be as near the critical value as it is today, it must have been 1 ± 10^{-60} at the Planck scale [14]. Therefore, $\Omega = 1$ is considered the natural value even in the non-inflationary case. If Ω is not equal to 1, then it will soon diverge rapidly from the critical value and we would be living in a special epoch. Since the amount of luminous matter is only of order $\Omega_{\text{lum}} < 0.01$, there must be a large amount of dark matter.

While it is clear that some portion of the universe is made up of dark matter, what form this dark matter takes is less certain. There is a long and diverse list

of candidates with a wide range of properties. These candidates can be divided into two types: baryonic and non-baryonic. Among the baryonic candidates are white dwarfs, brown dwarfs, black holes, Jupiter-sized planets, and neutron stars. All these objects would be classified as MACHOs. Recent searches for MACHOs using microlensing of distant stars in the galactic bulge and in satellite galaxies of the Milky Way have been successful in detecting some microlensing events [15, 16, 17]. In fact, the theoretical lower limit for baryonic matter from SBBN is somewhat *above* the amount of luminous matter observed [2], so the existence of MACHOs is not surprising. To remain consistent with SBBN, there must be some amount of baryonic dark matter.

However, it appears that baryonic dark matter cannot be *all* of the dark matter. Constructing models of the galaxy where MACHOs make up the entire dark matter halo is difficult in light of the observed number of microlensing events [18]. If primordial element abundances are calculated using $\Omega_b \sim 1$, deuterium is severely underproduced and helium-4 and lithium-7 are overproduced [2]. Even if $\Omega < 1$, the upper limit placed by SBBN on the amount of baryonic matter is well below the dynamical observations of Ω described above. A non-baryonic form of dark matter is needed to make up the difference. Similarly, theories of structure formation in which the mass density of the universe consists of mostly baryonic matter do not produce the amount of structure observed in the universe without large initial perturbations. These perturbations would show up as anisotropies in the cosmic microwave background. The lack of such anisotropies in the COBE observations of the microwave background suggests that some portion of the mass density must be non-baryonic [19].

Alternate explanations for the arguments given in favour of dark matter exist. The 3 K background radiation could be explained by grain-thermalized starlight with very massive population III stars generating the observed light element abundances

[20]. Difficulties with structure formation based on the smoothness of the CMBR are avoided, as are the limits on baryonic matter arising from SBBN. Models of inhomogenous nucleosynthesis might also provide a way of avoiding the baryonic matter limit [21]. There is observational evidence that some galactic clusters might have more baryonic matter than is allowed in SBBN [8, 20], but the interpretation of the observations remains open to debate.

2 Supersymmetry

Particle physics proposes several non-baryonic dark matter candidates, such as axions, massive neutrinos, and the lightest supersymmetric partners (LSP). This thesis is concerned with the neutralino, an LSP which arises out of supersymmetric grand unified theories that extend beyond the standard model of particle interactions.

2.1 The Standard Model of Particle Physics

The standard model of particle physics is a description of the known particles and forces (except gravity) in the universe. It is a gauge theory based on the symmetry group $SU(3) \times SU(2) \times U(1)$. There are three distinct forces within it: the strong, weak, and electromagnetic forces. The weak and electromagnetic forces are partially unified in $SU(2) \times U(1)$ electroweak theory [22, 23, 24], while the strong force is described by $SU(3)$ quantum chromodynamics [25, 26]. Despite being a theory grafted together from three distinct forces and symmetry groups, it has very successfully predicted experimental results to high precision.

A summary of the elementary particles in the model is given in Table 1. There are two main types of particles in the standard model: force-carrying bosons (integer spin particles) and fermions (spin- $\frac{1}{2}$ particles), the constituents of matter. The electroweak force is carried by the photon, Z boson, and W boson; the strong force by gluons. A scalar boson, the Higgs, arises from the broken symmetry of the electroweak theory. The Higgs has not yet been observed. Fermions are subdivided into quarks, which undergo strong interactions, and leptons, which do not. Each of the twelve elementary fermions has a corresponding antiparticle with the same mass and spin, but with opposite values for other properties such as charge. Fermions also come in three generations, each more massive than the previous. All the molecules and atoms that comprise ‘normal’ matter are made of particles from the first (lightest) generation.

	Name	Symbol	Mass (GeV)	Charge	Spin
1 st Generation	Electron	e	5.1×10^{-4}	-1	$\frac{1}{2}$
	Electron neutrino	ν_e	$< 7 \times 10^{-9}$	0	$\frac{1}{2}$
	Up quark	u	0.005	$+\frac{2}{3}$	$\frac{1}{2}$
	Down quark	d	0.01	$-\frac{1}{3}$	$\frac{1}{2}$
2 nd Generation	Muon	μ	0.1	-1	$\frac{1}{2}$
	Muon neutrino	ν_μ	$< 3 \times 10^{-4}$	0	$\frac{1}{2}$
	Charm quark	c	1.5	$+\frac{2}{3}$	$\frac{1}{2}$
	Strange quark	s	0.2	$-\frac{1}{3}$	$\frac{1}{2}$
3 rd Generation	Tau	τ	1.8	-1	$\frac{1}{2}$
	Tau neutrino	ν_τ	< 0.03	0	$\frac{1}{2}$
	Top quark	t	180	$+\frac{2}{3}$	$\frac{1}{2}$
	Bottom quark	b	4.7	$-\frac{1}{3}$	$\frac{1}{2}$
Bosons	Photon	γ	0	0	1
	W boson	W^\pm	80	± 1	1
	Z boson	Z^0	91	0	1
	Gluon	g	0	0	1
	Higgs boson	H	$\lesssim 1000$	0	0

Table 1: A summary of the elementary particles in the standard model.

For example, the proton (uud) and the neutron (udd) are bound states made from the first generation quarks.

The standard model contains a number of parameters whose values are not predicted by the theory. Many of these parameters are determined by experimental results. Fermion masses, for example, are measured experimentally and inserted by hand. 18 independent parameters, along with the $SU(3) \times SU(2) \times U(1)$ framework, complete the model.

2.2 Shortcomings of the Standard Model

In spite of the standard model's many successes, it is widely believed to be incomplete — a low-energy approximation of a more fundamental theory. There are many reasons for this belief, even though there is no unambiguous experimental evidence to contradict the standard model: there are the large number of free parameters that go into the model whose values are neither predicted nor constrained by the theory itself; there is no explanation for the existence of three generations of matter; there is no unification between quarks and leptons in the standard model, yet the electron and proton charges are equal to high precision; there are three coupling constants, g , g' , and g_s , corresponding to three separate forces that are not unified in the standard model; even the unification of the weak and electromagnetic forces in $SU(2) \times U(1)$ theory is only a partial unification that has two distinct forces, each with its own symmetry group and coupling constant. All of these are reasons to doubt the completeness of the standard model.

Another apparent shortcoming of the standard model appears in the naturalness (or hierarchy) problem. In the standard model there are four scalar (spin-0) Higgs particles postulated. Three Higgs particles are eaten by the W^\pm and Z bosons to generate their masses, and a fourth (yet to be observed) massive Higgs remains. These masses are related to the scale at which the $SU(2) \times U(1)$ theory is broken: the weak scale (~ 100 GeV, so $m_{\text{Higgs}} \propto 100$ GeV).

The standard model is a renormalizable field theory and could be valid at any energy scale Λ . At high energies, scalar particles naturally take on masses of order Λ through quadratically divergent quantum corrections (ie. $m_{\text{Higgs}}^2 = (m_{\text{Higgs}}^0)^2 + a\Lambda^2$). In effect, the scalars assume masses of order the highest energy scale Λ_{max} for which the theory is valid. It is widely expected that at some energy scale the standard model will break down, such as those scales suggested by Grand Unified Theories

(10^{16} GeV) or the Planck scale (10^{19} GeV). Because $m_{\text{Higgs}}^2 \propto \Lambda_{\text{max}}^2$, Higgs scalars should acquire masses of the same order through the quadratic corrections, masses far above the weak scale and contradictory to masses in the known particle spectrum. To preserve the weak scale the quadratic divergences must be fine tuned against a bare term to at least 28 decimal places [27]. This is the naturalness problem.

2.3 Supersymmetric Particle Spectrum

Many of these shortcomings can be addressed within the framework of a supersymmetric theory. (For reviews of supersymmetry, see [27, 28] and references therein). Supersymmetry (SUSY) is a symmetry between bosons, the particles that carry force, and fermions, the constituents of matter. In a sense it is a unification of matter and interaction. Supersymmetry is not an exact symmetry of nature. If it were, every particle would have a supersymmetric partner of identical mass. The symmetry must be broken and a doubling of the known particles is required in the simplest model (called the minimal supersymmetric standard model, or MSSM). All bosons are postulated to have a related supersymmetric fermion partner, and vice versa. The boson partners of fermions are named by placing an “s-” in front of the particle name. An electron, for example, has a related boson called the selectron. The supersymmetric partners of quarks are squarks. Bosons have fermion partners named by adding “-ino” to the end of the name. Photons have superpartners called photinos. A summary of particles in the MSSM is given in Table 2.

In the MSSM there are actually two squarks and two sleptons for each quark and lepton, one for the left-handed and one for the right-handed state of the fermion, although the number of degrees of freedom (2 for the spin- $\frac{1}{2}$ quark and one for each spin-0 squark) remains the same. The neutrino, which is (apparently) left-handed only, has a single partner. There is an additional Higgs doublet required, resulting in

Symbol	Standard particle	Symbol	Supersymmetric particle
q	quarks	\tilde{q}	squarks
u	up-type quark	\tilde{u}_L, \tilde{u}_R	up-type squark
d	down-type quark	\tilde{d}_L, \tilde{d}_R	down-type squark
l	leptons	\tilde{l}	sleptons
e	electron	\tilde{e}_L, \tilde{e}_R	selectron
ν	neutrino	$\tilde{\nu}$	sneutrino
g	gluons	\tilde{g}	gluinos
W^\pm	W boson	$\tilde{\chi}_1^\pm, \tilde{\chi}_2^\pm$	charginos
H^\pm	charged Higgs	\tilde{W}^\pm	w-ino
		\tilde{H}^\pm	charged higgsino
		$\tilde{\chi}_1^0, \tilde{\chi}_2^0, \tilde{\chi}_3^0, \tilde{\chi}_4^0$	neutralinos
γ	photon	$\tilde{\gamma}$	photino
Z^0	Z boson	\tilde{Z}	z-ino
$H_1^0 (H^0)$	heavy scalar Higgs	\tilde{B}	b-ino
$H_2^0 (h^0)$	light scalar Higgs	\tilde{W}_3	w-ino
$H_3^0 (A^0)$	pseudoscalar Higgs	\tilde{H}	neutral higgsino

Table 2: Standard particles and their supersymmetric partners. Alternate designations for the Higgs particles are given in brackets. The indented particles listed under the charginos and neutralinos are examples of names sometimes used when a particular chargino or neutralino (which is a mixture of states) is composed almost entirely of one state.

a total of five Higgs particles, instead of four in the standard model.

The names given for charginos and neutralinos in the table require some explanation. The supersymmetric partners of the W bosons and of the charged Higgs are generally called charginos. The chargino is actually a mixture of states, partially made from both the state corresponding to the partners of the W boson and of the charged Higgs. Depending on how a given supersymmetric model is constructed, the chargino could be made purely of either partner. In these cases the chargino is often called a w-ino (\widetilde{W}^\pm) or a charged higgsino (\widetilde{H}^\pm). The same is true for the photino ($\widetilde{\gamma}$), the z-ino (\widetilde{Z}), and the neutral higgsino (\widetilde{H}) in the case of neutralinos. The photon and Z boson are themselves made from a mixture of the B field and the W_3 field in the combined $SU(2) \times U(1)$ electroweak theory and neutralinos made purely of these states are also possible. These are included in the Table 2 as the b-ino (\widetilde{B}) and the w-ino (\widetilde{W}_3). Finally, since no other particle (normal or supersymmetric) uses the symbol χ the tilde is usually left out.

2.4 Benefits of Supersymmetry

Introducing superpartners for all particles solves the naturalness problem. The quantum corrections arising from fermions have the opposite sign to those from bosons. The contributions from a particle's superpartner cancel out the contributions from the particle itself, eliminating quadratic divergences.¹ The cancellation is not exact because the symmetry is broken, but as long as supersymmetric particle masses are below about 1 TeV the weak scale is preserved [29].

Another benefit of supersymmetry is its effect on grand unified theories (GUTs). Coupling 'constants' for the strong, weak, and electromagnetic forces are not constant, but vary with energy scale. As the energy scale probed increases the couplings ap-

¹When integrating over momenta up to the 'cut-off' Λ , divergences occur when the result contains terms $\propto \Lambda^{+n}$ or $\log \Lambda$, as opposed to convergences with terms $\propto \Lambda^{-n}$.

proach one another and might eventually have a common value at the unification scale. In some GUTs without supersymmetry, unification occurs at about 5×10^{14} GeV. Unification at this scale has implications for proton decay: it predicts rates faster than limits from current experiments. The extra particles in a supersymmetric theory slow the evolution of coupling constants so that unification does not occur until 2×10^{16} GeV. Proton decay is suppressed, allowing GUTs to remain consistent with current proton decay limits. In other GUTs, coupling constants do not unify at any scale without supersymmetry [30, 31].

Supersymmetry itself, of course, is not a complete theory of everything: some problems of the standard model still remain. The number of free parameters in a SUSY model is greater than in the standard model. While it is thought to help grand unified theories, there is no unification of forces inherent in the model, and quarks and leptons remain unrelated. Bearing this in mind, supersymmetry may be only the next step in developing a more complete picture of particle physics.

2.5 *R*-parity and the Neutralino

In supersymmetric models a new symmetry, *R*-parity, can be introduced. *R*-parity is defined by $R = (-1)^{3(B-L)+2S}$ for a particle of spin S , baryon number B and lepton number L .² The formula implies even *R*-parity ($R = 1$) for normal particles and odd *R*-parity ($R = -1$) for supersymmetric particles. Most models assume that *R* is conserved, a consequence of baryon-lepton invariance. Without *R* conservation, baryon and lepton number violating processes, like proton decay, are allowed at significant levels. Experimental limits on these processes severely constrain *R*-parity violating theories [32]. The introduction of *R*-parity conservation has an important consequence for dark matter: the lightest supersymmetric particle must be stable.

²The baryon number is 1 for baryons and -1 for antibaryons, or $\frac{1}{3}$ and $-\frac{1}{3}$ for individual quarks. Similarly, the lepton number is 1 for leptons (eg. e^- , ν_e) and -1 for antileptons (eg. e^+ , $\bar{\nu}_e$).

Consider, for example, the search at LEP (the Large Electron-Positron collider at CERN, Geneva) for charginos via pair production and decays in the process [33]

$$e^+e^- \rightarrow Z^0 \rightarrow \tilde{\chi}_1^+ \tilde{\chi}_1^- . \quad (2)$$

R -parity is a multiplicative symmetry, so $R = 1 \times 1 = 1$ for the left side of the equation. $R = 1$ for the Z boson, and $R = -1 \times -1 = 1$ for the two charginos produced. Supersymmetric particles are in general very unstable, and a chargino will immediately decay into lighter particles via processes such as

$$\tilde{\chi}_1^+ \rightarrow e^+ \tilde{\nu}_e . \quad (3)$$

R -parity is again conserved with $R = -1$ for the chargino and $R = 1 \times -1 = -1$ for the decay products. It is easy to see that whenever a supersymmetric particle decays, it must produce one (or an odd number) of supersymmetric particles to conserve R -parity. Eventually the chain of decays ends in the lightest supersymmetric particle: there are no lighter supersymmetric particles to decay into, and R -parity is violated if it decays entirely into normal particles. Usually the lightest superpartner is the least massive of the four neutralinos, often referred to as simply *the* neutralino. This particle is the best candidate for the weakly interacting massive particle (WIMP).

The superpartners of the gauge and Higgs bosons (gauginos and higgsinos) can mix. As a result, the physical mass eigenstates (charginos and neutralinos) are model-dependent linear combinations of these states. Diagonalizing the mass matrix for neutralinos yields the eigenstates of the system — the physically observable particles.

The mass matrix for neutralinos is

$$\begin{bmatrix} M_1 & 0 & -m_Z \cos \beta \sin \theta_W & m_Z \sin \beta \sin \theta_W \\ 0 & M_2 & m_Z \cos \beta \cos \theta_W & -m_Z \sin \beta \cos \theta_W \\ -m_Z \cos \beta \sin \theta_W & m_Z \cos \beta \cos \theta_W & 0 & -\mu \\ m_Z \sin \beta \sin \theta_W & -m_Z \sin \beta \cos \theta_W & -\mu & 0 \end{bmatrix} \quad (4)$$

where M_1 and M_2 are gaugino mass parameters, μ is the higgsino mass parameter, $\tan \beta = v_2/v_1$ is the ratio of vacuum expectation values of the Higgs fields, m_Z is the Z boson mass, and θ_W is the Weinberg angle. From this mass matrix, the lightest neutralino can be written as

$$\chi = N_1 \tilde{B} + N_2 \tilde{W}_3 + N_3 \tilde{H}_1^0 + N_4 \tilde{H}_2^0, \quad (5)$$

with N_i representing the coefficients arising from diagonalizing the matrix. This equation shows that the neutralino can be expressed as a mixture of states corresponding to the superpartners of the B and W_3 gauge fields (gauginos) and the H_1^0 and H_2^0 neutral Higgs bosons (higgsinos). The neutralino can be almost entirely gaugino or higgsino, or a mixture of both. This is quantified by the gaugino fraction [34]

$$f_g = |N_1|^2 + |N_2|^2. \quad (6)$$

The neutralino is primarily gaugino when $f_g > 0.5$ and primarily higgsino when $f_g < 0.5$.

Properties like the gaugino fraction vary with changes in the input parameters used to construct the supersymmetric model. Considerable effort has gone into detecting evidence for supersymmetry and reducing the allowed parameter space. It is here that astronomy plays an important role. A relic abundance of WIMPs in the universe could influence astrophysical processes, such as structure formation and stellar evolution, or it might allow for WIMP detection in high-energy neutrino telescopes. Since a supersymmetric particle is the primary candidate for the WIMP, detection of (or a failure to detect) WIMPs invariably leads to constraints on supersymmetry through the neutralino.

2.6 Relic Abundance

The high temperatures in the early universe would have allowed neutralinos to be created thermally. Lighter particles had sufficient kinetic energy to collide and cre-

ate heavier particles such as $\chi\bar{\chi}$ (neutralino-antineutralino) pairs. At the same time heavier particles could decay if they were unstable, or like $\chi\bar{\chi}$ pairs they could annihilate. As long as the temperature of the universe was greater than the neutralino mass the constant annihilation of particle pairs was balanced by their creation. Neutralinos were in thermal equilibrium at this time. As the universe expanded and cooled the temperature fell below the neutralino mass. It became more difficult to create $\chi\bar{\chi}$ pairs: they could only be created on the high energy tail of the distribution of particles. Annihilations continued while neutralinos remained in thermal equilibrium causing their number density to drop off exponentially $\propto \exp(-m_\chi/T)$ [35]. If neutralinos had remained in equilibrium until the present their number density would have been suppressed to the point where they would not contribute significantly to the density of the universe. However, as the universe continued its expansion and annihilations continued to reduce the number of neutralinos, a point was reached where the probability of $\chi\bar{\chi}$ pairs meeting became so small that annihilations effectively stopped. They fell out of equilibrium and a relic cosmological abundance remained.

The size of the relic abundance is determined by the thermally averaged cross section for neutralino annihilations $\langle\sigma_{Av}\rangle$. A larger cross section reduces the number of remaining neutralinos since annihilations are able to proceed for a longer period of time before the probability of $\chi\bar{\chi}$ pairs meeting becomes too small. This is shown in Figure 2, along with the strong suppression of neutralinos that would result if they remained in thermal equilibrium. The relic density of neutralinos is given approximately by [36]

$$\Omega_\chi \sim \frac{10^{-26} \text{ cm}^3 \text{ sec}^{-1}}{\langle\sigma_{Av}\rangle}. \quad (7)$$

The relic density can be altered by complicating factors. If there is a particle X , slightly heavier than the neutralino with a larger annihilation cross section, then the neutralino might convert to this particle and the neutralino abundance will actually be controlled by X in a process called coannihilation [37]. Changes in the entropy

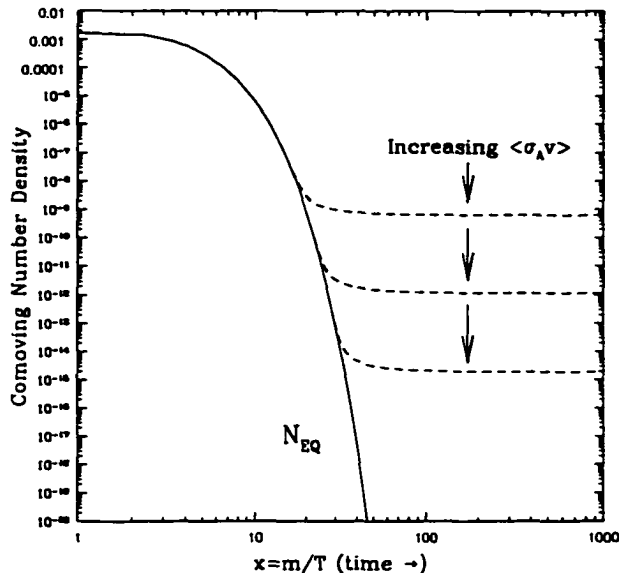


Figure 2: Comoving number density of neutralinos in the early Universe. The dashed curves are the actual abundance, and the solid curve is the equilibrium abundance. From [1].

of the universe, perhaps resulting from a phase transition, can also alter the relic abundance [1]. These special cases aside, equation (7) is a valid approximation. Using the annihilation cross section³ for weak scale interactions

$$\langle\sigma_A v\rangle \sim \alpha^2(100 \text{ GeV})^{-2} \sim 10^{-25} \text{ cm}^3 \text{ sec}^{-1} \quad (8)$$

remarkably leads to a value for $\Omega_\chi \sim 1$. The neutralino, by its weakly interacting nature, is a natural candidate for dark matter. The fact that a particle postulated to exist as a solution to problems within the standard model has the very characteristics needed to (potentially) solve the dark matter problem is viewed as a compelling argument in favour of neutralinos.

³Natural units, where factors of \hbar and c convert quantities to common units, are often used for convenience. The annihilation cross section can be expressed in $\text{cm}^3 \text{ sec}^{-1}$ or in GeV^{-2} by multiplying by $\hbar^2 c^3$. Particle masses are commonly given in GeV/c^2 , or simply GeV using the convention $\hbar = c = 1$.

There is a key difference between the process described above and the one that left baryonic matter in the universe. Neutralinos are what are known as Majorana particles: they are their own anti-particles. For Dirac particles with a particle-antiparticle asymmetry, the relic abundance is usually determined by that asymmetry, not by freeze out from thermal equilibrium [38]. The discussion above would also change dramatically for a particle with a different interaction strength, such as a gravitino or axino that arises from models extending beyond the MSSM.

With a thermal relic population of neutralinos left in the universe, modelling structure formation becomes easier. The most successful models of structure formation assume the universe contains cold dark matter, like the neutralino. Models with only baryonic matter are unable to produce structure in the universe without large fluctuations in the CMBR - fluctuations that contradict the observed CMBR smoothness [39]. It is possible that a model with only baryons might eventually be found that is able to produce structure without these fluctuations, but at present none exists.

3 Indirect Detection of Neutralinos

If neutralinos are indeed present in the universe, it may be possible to detect them indirectly using high-energy neutrino detectors/telescopes. Although it is weakly interacting, a neutralino may still scatter and become trapped in the gravitational well of an astronomical body like the Sun or Earth. As it settles into the centre of the body through further scattering, the probability increases that it will collide with another neutralino and annihilate. The by-products of such an annihilation include high-energy neutrinos.

Indirect detectors typically work by observing Čerenkov light from muons. When a high-energy neutrino interacts with the material surrounding the detector, a muon can be produced. As the muon travels through the medium of the detector, usually water, it emits Čerenkov light that is observed by photomultiplier tubes. Timing when the light reaches each photomultiplier allows the path of the muon to be reconstructed. The detectors do not attempt to measure high-energy neutrinos directly because there would be too few interactions within the relatively small confines of the detection medium and the photomultiplier tubes. By using muons, all the rock surrounding a detector becomes the target for neutrino interactions and more events are possible.

Reducing the background from cosmic ray muons is achieved by placing detectors below the surface of the Earth. Even with detectors placed far underground, there is still a large flux of cosmic ray muons travelling down through the rock. This background can be dealt with by counting only upward-going muon events. Observations of the Sun, therefore, are only possible when it is below the horizon. One detector that has operated for a number of years is the Kamiokande detector, located in the Kamioka mine in Japan under an equivalent of 2700 m of water [40]. This experiment, along with the Irvine-Michigan-Brookhaven (IMB) detector which is no longer operational, has already placed an upper limit of $2.1 \times 10^{-2} \text{ m}^{-2}\text{yr}^{-1}$ events from the

Sun [41, 42, 43]. A similar limit from Kamiokande of $1.3 \times 10^{-2} \text{ m}^{-2}\text{yr}^{-1}$ applies to the Earth.

A new generation of detectors is coming on line or being planned. Among these are DUMAND (Deep Underwater Muon And Neutrino Detector), which will use strings of photomultiplier tubes anchored to the deep ocean floor off of Hawaii, and AMANDA (Antarctic Muon And Neutrino Detector), which will use arrays of photomultipliers placed deep in the clear Antarctic ice sheet. The next generation of detectors will be sensitive down to event rates of roughly $10^{-4} \text{ m}^{-2}\text{yr}^{-1}$ [44]. If an unambiguous signal of high-energy neutrinos is eventually detected, an important goal will be determining the properties of the neutralino. Doing that goes to the heart of revealing the nature of the underlying supersymmetry.

To investigate the possibility of determining neutralino properties from the high-energy neutrinos produced by neutralino annihilation, a simulation of event rates for a range of MSSM input parameters was carried out. A detailed description of the entire process will be given below, but the general procedure is this: a supersymmetric model is constructed, determining the properties of the neutralino; important quantities, such as the relic abundance, are also calculated using model information and inputs from physics and astrophysics; the capture rate for the Sun and Earth can then be determined using these quantities along with the neutralino's properties; the rate of annihilation is calculated, and by modelling the subsequent decay of annihilation products the flux of high-energy neutrinos is determined; the effects of neutrino interaction with the solar medium are included because of the Sun's mass and density; finally, the flux of neutrinos is converted into a muon event rate for a detector.

Jungman, Kamionkowski, and Griest [45, 27] have developed computer code called `Neutdriver` to perform many of these calculations. The program takes a set of input parameters and builds a supersymmetric model, producing detailed information about

the resulting neutralino. The program also outputs information needed to find the rate of muon events in a neutrino detector, including an approximate calculation of event rates created using a Monte Carlo simulation for the Kamiokande detector [40]. Instead of using `Neutdriver`'s approximation for the event rate, `Mathematica` code was developed to calculate event rates based on the model information supplied by `Neutdriver` and analytic expressions for the neutrino spectrum produced by $\chi\bar{\chi}$ annihilation.

3.1 Supersymmetric Models

The properties of a neutralino depend on the supersymmetric model. A wide range of input physics and free parameters go into a model and ultimately determine the masses, cross sections, decay channels, and other physical properties of the neutralino and the rest of the supersymmetric particles. The most general form of the supersymmetric model has over 60 input parameters. Much of this parameter space is physically uninteresting or produces results that are excluded by other constraints, so a subset of the parameter space is explored [27].

Table 3 is a summary of the parameter space examined using `Neutdriver`'s `Practical` model. Five input parameters are used: M_2 is one of three gaugino mass parameters; $\tan\beta = v_2/v_1$ is the ratio of Higgs vacuum expectation values; $m_{H_3^0}$ is the mass of the pseudoscalar Higgs and it, together with $\tan\beta$, determines the Higgs boson spectrum; μ is the Higgsino mass scale; and M_Q^2 determines the mass scale for squarks and sleptons. Other mass-squared parameters are given the same value as M_Q^2 . The parameter space is reduced by making common GUT assumptions. For example, the gaugino mass parameter M_1 is related to M_2 by [46]

$$M_1 = \frac{5}{3} \tan^2 \theta_W M_2. \quad (9)$$

Other parameters, such as soft supersymmetry breaking parameters A_τ , A_b , and A_t .

are assumed to be zero to simplify calculations. Many parameters are only relevant in the context of supergravity models and are not needed in an examination of the MSSM. In all models, 180 GeV is used for the top quark mass.

Parameter	Lower Value	Upper Value
M_2	15 GeV	3000 GeV
$m_{H_3^0}$	170 GeV	470 GeV
μ	-1000 GeV	1000 GeV
$\tan \beta$	2	22
$M_{\tilde{Q}}^2$	$4 \times 10^4 \text{ GeV}^2$	10^6 GeV^2

Table 3: Range of MSSM parameters explored.

The ranges selected for these five parameters are chosen so that the models produce good dark matter candidate without violating other experimental constraints. Nonetheless, many models will still end up being eliminated for failing to meet those criteria. Even after choosing what is hoped is a reasonable model parameter space to explore, it is still necessary to check each model individually to ensure no constraints have been violated. All of the constraints used are listed in the following section and summarized in Table 4.

3.2 Constraints

The relic abundance of neutralinos can be used as a simple constraint on supersymmetric models. The exact value of the total mass density Ωh^2 for the universe is uncertain, but it can not be greater than 1. If it were, the current rate of expansion would mean the universe is younger than 10 billion years old for $h \geq 0.4$, younger than the age of the oldest clusters [47]. Obviously, if $\Omega h^2 \leq 1$, the relic abundance of neutralinos $\Omega_\chi h^2 \leq 1$.

Constraint	Source
$\Omega_\chi h^2 \leq 1$	Expansion rate / age of universe
$m_{H_3^0} > 39 \text{ GeV}$ $m_{H_2^0} > 44 \text{ GeV}$	Higgs boson searches
$m_{\tilde{\chi}^\pm} > 62 \text{ GeV}$	$e^+e^- \rightarrow \tilde{\chi}^+\tilde{\chi}^-$ chargino searches
$m_\chi > 15 \text{ GeV}$	Z boson invisible width
$Z^0 \rightarrow \chi_0\chi_0 < 10^{-5}$ $Z^0 \rightarrow \chi_i\chi_j < 2 \times 10^{-3}$	Branching ratios for rare processes
$\Gamma_{\tilde{\chi}^\pm} < 2.1 \times 10^{-1} \text{ m}^{-2}\text{yr}^{-1}$ $\Gamma_{\tilde{\chi}^0} < 1.3 \times 10^{-1} \text{ m}^{-2}\text{yr}^{-1}$	Ruled out by current experiments
$\Gamma_{\tilde{\chi}^\pm}$ or $\Gamma_{\tilde{\chi}^0} > 10^{-5} \text{ m}^{-2}\text{yr}^{-1}$	Undetectable in upcoming experiments
Vacuum expectation values of scalar fields (except Higgs) vanish	Color / charge conservation
LSP is neutralino	—

Table 4: Constraints used to eliminate SUSY models. (References in text).

A lower limit on the relic density arises from the assumption that neutralinos make up the entire dark halo of our galaxy. The rate of neutralino capture is directly proportional to their local halo density. Assuming the local halo density $\rho_{\text{halo}} \approx 0.3 \text{ GeV cm}^{-3}$ is made entirely of neutralino dark matter ($\rho_\chi = \rho_{\text{halo}}$), the range of allowed values for their relic universal density is $0.025 < \Omega_\chi h^2 < 1$. Models with relic densities below this range do not contain enough neutralinos to make up the entire halo. It is possible that a neutralino with a small, cosmologically unimportant relic abundance could produce a detectable flux of high-energy neutrinos. While this is not a very satisfying situation, since it might leave the dark matter question unanswered, the models are not excluded. Scenarios where MACHOs are the dominant component of the local dark matter halo, although unlikely, are still viable [18]. Because of this, even models with $\Omega_\chi h^2 < 0.025$ are kept. Relic densities below this value, where the halo is partly or mostly something besides neutralinos, require scaling the local

neutralino density accordingly to keep capture rates from being inflated. The relation

$$\rho_\chi = \rho_{\text{halo}} \frac{\Omega_\chi h^2}{0.025} \quad (10)$$

is used for the scaling [44].

Accelerator searches for evidence of supersymmetry have not detected any particles beyond those in the standard model, but they have provided limits on particle masses and other properties. Searches for Higgs bosons have placed lower limits on Higgs masses of $m_{H_3^0} > 39$ GeV and $m_{H_2^0} > 44$ GeV [46]. A theoretical upper limit of $m_{H_2^0} < m_Z$ arises from the MSSM; further analysis that included radiative (quantum) corrections raised this to $m_{H_2^0} < 130$ GeV [27]. Chargino masses have also been constrained through searches for $e^+e^- \rightarrow \tilde{\chi}^+\tilde{\chi}^-$. The lower limit is $m_{\tilde{\chi}^\pm} > 62$ GeV [46].

A further requirement of any model is that the lightest supersymmetric particle be the neutralino. Having a stable relic that is charged or that is not weakly interacting makes for a very bad WIMP.

Mass limits for the neutralino are calculated by examining the Z boson's invisible width in accelerator experiments. This is the contribution to the Z boson cross section from processes that can not be measured directly in the accelerator. These processes are inferred by comparing experimental results to predictions from the standard model. These limits are extremely model dependent; a conservative lower bound of $m_\chi > 15$ GeV was adopted [46]. Branching ratios⁴ for rare processes involving Z bosons and all four neutralinos are also used to eliminate models. The upper limits on branching ratios for $Z^0 \rightarrow \chi_0\chi_0$ and $Z^0 \rightarrow \chi_i\chi_j$ are 10^{-5} and 2×10^{-3} respectively [48].

Electroweak symmetry breaking is caused by Higgs fields acquiring vacuum expectation values v_1 and v_2 , the values that define $\tan\beta$. A requirement of each

⁴The branching ratio represents the fraction of all decays that go through a particular path.

supersymmetric model is that the vacuum expectation values of all other scalar fields vanish, avoiding vacuum states that would break color or electric charge conservation [37].

A relic abundance of supersymmetric particles could have an effect on processes within a star. A neutralino might effectively reduce opacity and increase energy transport as it moves with relative ease between the core and outer regions of the stellar interior. This scenario was considered as a possible solution to the solar neutrino problem and as a way to resolve differences between observed and theoretical values for the normalized frequency separations of low-degree solar p-modes [49, 50, 51, 52, 53, 54]. Increased energy transport lowers the core temperature where nuclear reactions occur and thus reduces the number of solar neutrinos produced, at the same time as altering the frequency separation between low-degree p-modes that penetrate to the core. However, as solar models improved, the differences between observed and theoretical values for the frequency separation disappeared, and the addition of WIMPs worsened the agreement [55, 56, 57]. The WIMPs considered had masses around 5 GeV, lighter than the masses used here. Heavier WIMPs are unable to transport energy from the core efficiently and do not alter the solar interior significantly. The effect of WIMPs on later stages of stellar evolution has also been examined. In horizontal-branch stars, light (< 8 GeV) WIMPs are ineffective in energy transport, while heavier WIMPs are too centrally concentrated to alter stellar evolution [58].

Finally, direct and indirect detector experiments can constrain particle dark matter by eliminating models that would have been detected experimentally. Direct detectors try to measure the occasional interactions that occur when WIMPs pass through matter. For example, a germanium crystal detector can measure the slight temperature change caused by a neutralino colliding with an atom and depositing energy. Detectors like this have already placed strong limits on some forms of dark matter, such as Dirac neutrinos, and a new generation of detectors will, if they fail

to find evidence of neutralinos, further constrain neutralino parameter space [59]. Indirect detectors, as mentioned earlier, have been running for several years without detecting neutralinos. Any model that produces an event rate great enough that it would have been detected by past or present detectors is removed. Since there are large uncertainties in the event rate, the upper limit is increased by an order of magnitude to $\Gamma_{\odot} < 2.1 \times 10^{-1} \text{ m}^{-2}\text{yr}^{-1}$ solar events ($\Gamma_{\oplus} < 1.3 \times 10^{-1} \text{ m}^{-2}\text{yr}^{-1}$ for the Earth) to ensure models near the threshold of present day detectability are kept. A further reduction is made by removing models where the event rate for both the Sun and Earth is significantly below the threshold of the next generation of detectors, $10^{-4} \text{ m}^{-2}\text{yr}^{-1}$. Again, to keep the cuts conservative, event rates an order of magnitude below this value, down to $10^{-5} \text{ m}^{-2}\text{yr}^{-1}$, are kept.

The model parameter space explored represents nearly 100000 individual supersymmetric models. Removing models that have color- and charge-breaking vacua, a particle other than the neutralino as the lightest superpartner, or with $\Omega h^2 > 1$, leaves 34787 models. Applying the remaining constraints further reduces the number of models to 21768. Figure 3 shows the M_2 versus μ plane of parameter space after all cuts were made.

3.3 Capture in the Sun and Earth

The basic concept of neutralino capture is relatively simple. If a neutralino moving with some velocity v scatters off an astronomical object to a velocity less than v_{escape} , it is captured [60]. The neutralino settles into the centre of the object where it can annihilate with other captured neutralinos. Gould [61, 62, 63, 64, 65] has carried out detailed analysis of neutralino capture in the Sun and Earth. Given the factor of two uncertainty in the local halo mass density, the large uncertainty in the velocity dispersion of dark matter particles, and the model uncertainty in the fundamental

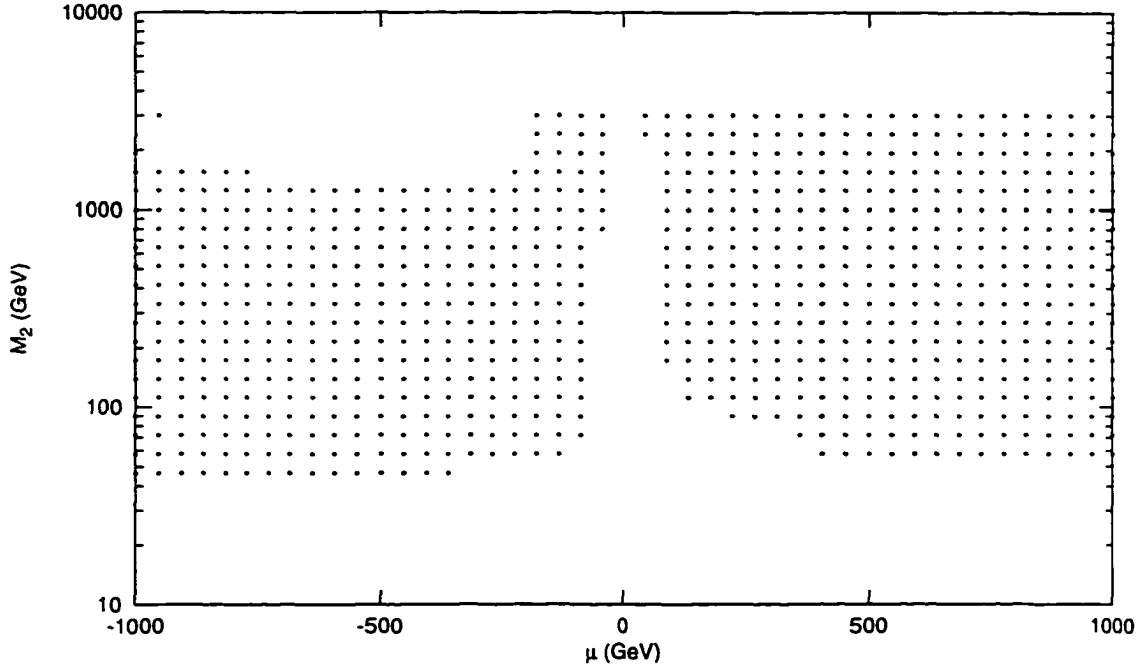


Figure 3: M_2 versus μ plane of parameter space after models that violate constraints are removed.

neutralino-nucleus elastic scattering cross section, approximations for the capture rate described in [27] can be used.

Calculations of neutralino capture in the Earth are not changed by the fact that the Earth is orbiting in the Sun's gravitational well. Free space is a valid approximation in this case [64]. Neutralino evaporation — where a neutralino scatters and is given a velocity boost that ejects it from the Sun or Earth — is insignificant for neutralinos with masses more than about 10 GeV [62].

3.4 $\chi\bar{\chi}$ Annihilation and Determining Event Rates

Once the capture rate is known, the rate of neutralino annihilation can be found. The equation for the evolution of the number of neutralinos in the Sun or Earth is

$$\frac{dN}{dt} = C - C_A N^2 - C_E N \quad (11)$$

where C is the capture rate and C_E is the rate of evaporation, which can be set to zero. The middle term is twice the annihilation rate, $\Gamma_A = C_A N^2/2$. C_A depends on the distribution of neutralinos and the annihilation cross section. Solving the equation for $N(t)$, the annihilation rate is then given by

$$\Gamma_A = \frac{C}{2} \tanh^2 \left(\frac{t}{\tau} \right). \quad (12)$$

τ represents the time required for capture and annihilation to reach equilibrium.

Neutralino annihilations do not directly produce energetic neutrinos; they come from the subsequent decay of the annihilation products. Several decay channels contribute to the flux of neutrinos and each is discussed in more detail below. Typically, high-energy neutrinos come from unstable particles that decay almost immediately after they are created. Longer lived particles interact with the surrounding medium and lose energy before they decay. This means electrons, muons, and light hadrons (up, down and strange quarks) do not contribute to the flux of high-energy neutrinos.

A high-energy neutrino detector actually measures events caused when neutrinos interact with the rock surrounding a detector, producing muons. The number of neutrino-induced muons passing through the detector is

$$\Gamma_{\text{detect}} = (1.27 \times 10^{-29} \text{ m}^{-2} \text{ yr}^{-1}) \frac{2\Gamma_A}{\text{sec}^{-1}} \left(\frac{m_\chi}{\text{GeV}} \right)^2 \sum_i a_i b_i \sum_F B_F \langle N z^2 \rangle_{F,i} \quad (13)$$

for neutrinos produced in the Sun [66]. The expression does not take into account the fact that observations of the Sun can only occur while it is below the horizon. Multiplying the expression by the square of the ratio of the Earth-Sun distance to the Earth's radius, 5.6×10^8 , gives the rate for the Earth. The first sum is over neutrinos of type i (neutrino or anti-neutrino). Differences between the interactions of a neutrino and an anti-neutrino require separate treatment for each type. The coefficients a_i and b_i model the production and propagation of muons in the rock surrounding the detector. The muon scattering coefficients are $a_\nu = 6.8$ and $a_{\bar{\nu}} = 3.1$. The muon range coefficients are $b_\nu = 0.51$ and $b_{\bar{\nu}} = 0.67$ [67].

When neutralinos annihilate, they can produce wide range of possible final states F . The second sum is over all the decay channels and B_F is the branching fraction for each channel. The branching fractions vary with the properties of the neutralino and must be calculated for each model. The relevant decay channels for $\chi\bar{\chi}$ annihilation are into quarks ($b\bar{b}$, $c\bar{c}$, and $t\bar{t}$), $\tau\bar{\tau}$, $W^\pm\bar{W}^\mp$, $Z\bar{Z}$, and channels with Higgs bosons (ZH_1^0 , ZH_2^0 , $W^\pm H^\mp$, $H_1^0 H_3^0$, and $H_2^0 H_3^0$).

$\langle Nz^2 \rangle$ is the second moment of the neutrino spectrum. The first variable N is simply the total yield of neutrinos. The second variable is the scaled energy, which is the energy of the neutrino divided by the injection energy given to it by the parent particle, or $z = E_\nu/E_{\text{in}}$. The second moment of the neutrino energy spectrum is calculated because the cross section for muon production in rock and the range of the muon are both proportional to neutrino energy, so the probability of producing a muon event that passes through the detector is proportional to the energy squared.

The Sun's density is great enough that neutrinos and antineutrinos produced in the core of the Sun will interact with the solar medium. Energy is lost through neutral current interactions, and neutrinos are absorbed through charged current interactions. A neutrino of type i injected into the Sun can be modelled to escape with energy

$$E_f = \frac{E_{\text{in}}}{1 + E_{\text{in}}\tau_i} \quad (14)$$

and probability

$$P_f = \left(\frac{1}{1 + E_{\text{in}}\tau_i} \right)^{\alpha_i}. \quad (15)$$

The parameters $\tau_\nu = 1.01 \times 10^{-3}$ GeV and $\tau_{\bar{\nu}} = 3.8 \times 10^{-4}$ GeV account for neutral current energy losses; $\alpha_\nu = 5.1$ and $\alpha_{\bar{\nu}} = 9.0$ are used when finding the escape probability of the neutrino [67]. These parameters appear in the second moment equations given below. Since the parameters are different for neutrinos and antineutrinos, the second moments from each type of neutrino will be different for the Sun. The Earth is not dense enough to affect neutrino propagation. Finally, in all cases where neu-

tralinos annihilate into particle-antiparticle pairs, the injection energy E_{in} is simply the neutralino mass $m_{\tilde{\chi}}$.

The following subsections describe the analytic expressions for the neutrino second moments needed in the event rate equation. All of the relevant decay channels ($b\bar{b}$, $c\bar{c}$, $t\bar{t}$, $\tau\bar{\tau}$, $W^\pm\bar{W}^\mp$, $Z\bar{Z}$, ZH_1^0 , ZH_2^0 , $W^\pm H^\mp$, $H_1^0 H_3^0$, and $H_2^0 H_3^0$) are listed. The expressions are accurate to about $\pm 10\%$, a level of uncertainty that is small compared to sources of error like the local halo density. The analytic treatments for the neutrino second moments in the following subsections were derived by Jungman and Kamionkowski [68].

3.4.1 Charm and bottom quark decay

A bottom or charm quark injected into the Earth by neutralino annihilation undergoes hadronization, an evolution into baryons and mesons. During this process, kinetic energy from a quark is converted into quark-antiquark pairs. The result is clusters of quarks and gluons with no net color that form hadrons moving in the same direction as the quark. Every time a quark-antiquark pair is produced, the energy of the original quark is reduced. A quark injected with energy E_{in} will have its energy reduced to $E_d = z_f E_{\text{in}}$ through hadronization, where $z_f = 0.58$ for c quarks and 0.73 for b quarks. The expression for the c quark second moment from the Earth is

$$\langle N z^2 \rangle_{c\bar{c}}^\oplus(E_{\text{in}}) = \frac{2z_f^2 \Gamma_{c \rightarrow \mu\nu X}}{15} \left(1 + \frac{\beta^2}{3} \right), \quad (16)$$

where $\Gamma_{c \rightarrow \mu\nu X} \simeq 0.13$ is the branching ratio for inclusive semileptonic decay of the c quark into muons. The velocity of the quark when it decays is $\beta = (1 - m_{\text{quark}}^2/E_d^2)^{1/2}$. The expression for the b quark is similar,

$$\langle N z^2 \rangle_{b\bar{b}}^\oplus(E_{\text{in}}) = \frac{z_f^2 \Gamma_{b \rightarrow \mu\nu X}}{10} \left(1 + \frac{\beta^2}{3} \right), \quad (17)$$

with $\Gamma_{b \rightarrow \mu\nu X} \simeq 0.103$.

A bottom or charm quark injected into the Sun also undergoes hadronization. As in the Earth, the energy of the quark is reduced to $E_0 = z_f E_{\text{in}}$. The greater density at the core of the Sun means an injected hadron interacts with the solar medium and loses energy before it decays and produces neutrinos. The final energy a hadron has when it decays, E_d , is picked from a decay distribution. The average value of E_d is

$$\langle E_d \rangle(E_0) = E_c \exp\left(\frac{E_c}{E_0}\right) \times \int_{\frac{E_c}{E_0}}^{\infty} \left(\frac{e^{-y}}{y}\right) dy \quad (18)$$

and the rms value is

$$\sqrt{\langle E_d^2 \rangle} = \sqrt{E_c(E_0 - \langle E_d \rangle)}. \quad (19)$$

As the energy of the injected hadron is increased, it becomes more likely that it will be stopped before it decays. Above energy $E_c = 250$ GeV for c quarks and $E_c = 470$ GeV for b quarks, the parent hadron is unlikely to decay before being stopped.

Using these equations, the second moment for c and b quarks channels is expressed as

$$\langle Nz^2 \rangle_{f,i}^{\odot}(E_{\text{in}}) \simeq \frac{\langle E_d \rangle^2}{E_{\text{in}}^2} h_{f,i} \left(\sqrt{\langle E_d^2 \rangle} \tau_i \right) \quad (20)$$

where $h_{f,i}(y)$ for c quarks is

$$h_{c,\nu_\mu}(y) = \frac{1}{180} \frac{32 + 25y + 5y^2}{(1+y)^5} \quad (21)$$

$$h_{c,\bar{\nu}_\mu}(y) = \frac{1}{7560} \frac{1344 + 3186y + 3834y^2 + 2786y^3 + 1242y^4 + 315y^5 + 35y^6}{(1+y)^9} \quad (22)$$

and for b quarks is

$$h_{b,\nu_\mu}(y) = \frac{1}{30} \frac{4+y}{(1+y)^4} \quad (23)$$

$$h_{b,\bar{\nu}_\mu}(y) = \frac{1}{1260} \frac{168 + 354y + 348y^2 + 190y^3 + 56y^4 + 7y^5}{(1+y)^8}. \quad (24)$$

3.4.2 τ lepton decay

The second moments for τ lepton decay are simpler than those for c and b quarks because there is no hadronization. For τ leptons injected into the Earth with velocity

$\beta = (1 - m_\tau^2/E_{\text{in}}^2)^{1/2}$. the second moment is

$$\langle Nz^2 \rangle_{\tau\bar{\tau}}^{\oplus}(E_{\text{in}}) = \frac{\Gamma_{\tau \rightarrow \mu\nu\nu}}{10} \left(1 + \frac{\beta^2}{3} \right), \quad (25)$$

where $\Gamma_{\tau \rightarrow \mu\nu\nu} \simeq 0.18$.

For neutrinos from τ lepton decay in the Sun,

$$\langle Nz^2 \rangle_{\tau\bar{\tau},i}^{\oplus}(E_{\text{in}}) = \Gamma_{\tau \rightarrow \mu\nu\nu} h_{\tau,i}(E_{\text{in}}\tau_i) \quad (26)$$

where the $h_{\tau,i}(y)$ function is the same as the one used for b quarks.

3.4.3 Top quark decay

Top quarks injected into the Sun and Earth decay almost exclusively into W bosons and b quarks. The second moment for the Earth is

$$\langle Nz^2 \rangle_{t\bar{t}}^{\oplus}(E_{\text{in}}) = \left(1 + \frac{\beta^2}{3} \right) \left(\frac{\Gamma_{W \rightarrow \mu\nu} E_W^2}{4m_t^2} \left[1 + \frac{1}{5}\beta_W^2(2 - f_L) \right] + \Gamma_{b \rightarrow \mu\nu} \frac{2z_f^2 E_b^2}{15m_t^2} \right). \quad (27)$$

The energy of the W boson in the frame of the decaying top is $E_W = (m_t^2 + m_W^2)/(2m_t)$; for the b quark it is $E_b = (m_t^2 - m_W^2)/(2m_t)$. The W boson velocity is $\beta_W = E_b/E_W$. The fraction of W bosons from top quark decay produced in the longitudinal helicity state is given by $f_L = (1 + 2m_W^2/m_t^2)^{-1}$. (Reference [27] has m_W and m_t reversed in this expression. The correct form is found in [68]).

Determining $\langle Nz^2 \rangle$ for top quarks in the Sun is somewhat complicated, involving the integration of the b quark and W boson second moments for the Sun over the injection energy of the b quark and W boson from top decay. At first, this integration was used in the `Mathematica` code developed. To make the code more efficient, an analytic fit created by Jungman and Kamionkowski [68] to approximate $\langle Nz^2 \rangle_{t\bar{t}}^{\oplus}$ replaced the integration. The analytic fit

$$\log_{10} \left[\langle Nz^2 \rangle_{t\bar{t},i}^{\oplus} \right] = A_i (\log_{10} E_{\text{in}})^2 - B_i (\log_{10} E_{\text{in}}) + C_i \quad (28)$$

is accurate to within 10% over the energy range $m_t \leq E_{\text{in}} \leq 3000$ GeV. The coefficients are $A_\nu = -0.825$, $A_{\bar{\nu}} = -0.889$, $B_\nu = -3.31$, $B_{\bar{\nu}} = -2.94$, $C_\nu = -5.39$ and $C_{\bar{\nu}} = -6.40$. Note that top quarks decay immediately, so that unlike the case for c and b quarks, the dense solar medium does not reduce the energy of top quarks before they decay.

3.4.4 W and Z boson decay

W and Z bosons decay directly into neutrinos. They also decay into quarks which then produce neutrinos, but these neutrinos have lower energies and are not important for the calculation of muon events. The second moment for neutrinos from W^+W^- pairs in the Earth is

$$\langle Nz^2 \rangle_{W^+W^-}^\oplus(E_{\text{in}}) = \Gamma_{W \rightarrow \mu\nu} \frac{1}{4} \left(1 + \frac{2}{5} \beta^2 \right) \quad (29)$$

where $\Gamma_{W \rightarrow \mu\nu} = 0.105$ is the branching ratio for W decay into muon neutrinos and $\beta = (1 - m_W^2/E_{\text{in}}^2)^{1/2}$ is the velocity of the injected W boson. The equation for Z bosons is

$$\langle Nz^2 \rangle_{ZZ}^\oplus(E_{\text{in}}) = 2\Gamma_{Z \rightarrow \nu_\mu \bar{\nu}_\mu} \frac{1}{4} \left(1 + \frac{2}{5} \beta^2 \right) \quad (30)$$

with the branching ratio for Z bosons into muon neutrinos $\Gamma_{Z \rightarrow \nu_\mu \bar{\nu}_\mu} = 0.067$ and velocity $\beta = (1 - m_Z^2/E_{\text{in}}^2)^{1/2}$.

For the Sun, the effects of energy loss and stopping of neutrinos are once again taken into account. The second moment for W bosons is

$$\langle Nz^2 \rangle_{W^+W^-}^\oplus(E_{\text{in}}) = \frac{\Gamma_{W \rightarrow \mu\nu}}{\beta} \frac{2 + 2E\tau_i(1 + \alpha_i) + E^2\tau_i^2\alpha_i(1 + \alpha_i)}{E_{\text{in}}^3\tau_i^3\alpha_i(\alpha_i^2 - 1)(1 + E\tau_i)^{\alpha_i+1}} \Bigg|_{E=E_{\text{in}}(1+\beta)/2}^{E=E_{\text{in}}(1-\beta)/2} \quad (31)$$

The equation for Z bosons is obtained by replacing $\Gamma_{W \rightarrow \mu\nu}$ with $2\Gamma_{Z \rightarrow \nu_\mu \bar{\nu}_\mu}$. (Note that the upper and lower limits of evaluation in this equation are given correctly in [66], but are reversed in [68] and [27]).

3.4.5 Higgs and Higgs-gauge boson decay

There are five channels important for muon event rate calculations that involve the decay of Higgs bosons: ZH_1^0 , ZH_2^0 , $W^\pm H^\mp$, $H_1^0 H_3^0$, and $H_2^0 H_3^0$ [44]. Often, only the contributions from Z and W bosons are considered in Higgs-gauge boson channels, and Higgs-Higgs channels are ignored. Since Higgs decay can sometimes make significant contributions to the high-energy neutrino flux, all of the Higgs decays are included here for completeness. The Higgs and gauge bosons produced in neutralino annihilation have different masses, so it is no longer valid to use the simple relation $E_{\text{in}} = m_\chi$. The energy given to each particle created when a neutralino annihilates is

$$E_1 = \frac{4m_\chi^2 + m_1^2 - m_2^2}{4m_x} \quad E_2 = \frac{4m_\chi^2 + m_2^2 - m_1^2}{4m_x}. \quad (32)$$

The second moment for annihilation channels involving Higgs-gauge boson final states in the Earth is

$$\langle N z^2 \rangle_{ZH}^\oplus = \Gamma_{Z-\nu_\mu \bar{\nu}_\mu} \frac{1}{4} \left(1 + \frac{1}{5} \beta_Z^2 \right) + \text{Higgs decay contribution}. \quad (33)$$

The first part of the equation is the contribution from the gauge boson. This applies to ZH_1^0 and ZH_2^0 , as well as $W^\pm H^\mp$ by replacing $\Gamma_{Z-\nu_\mu \bar{\nu}_\mu}$ with $\Gamma_{W-\mu\nu}$ and velocity $\beta_Z = (1 - m_Z^2/E_Z^2)^{1/2}$ with β_W . E_Z and E_W are found by using equation (32).

The equation for the Sun is

$$\langle N z^2 \rangle_{ZH}^\ominus = \frac{\langle N z^2 \rangle_{ZZ}^\ominus}{2} + \text{Higgs decay contribution}. \quad (34)$$

The second moment for Z bosons given here is simply the one used earlier for Z boson decay, divided by two since there is now only one Z boson. The second moment for $W^\pm H^\mp$ is similar, except the second moment for W bosons is used instead. The energy of the injected gauge boson, E_Z or E_W , is given by equation (32).

The Higgs decay contribution in equations (33) and (34) is the contribution from the decay of Higgs bosons into c quarks, b quarks, τ leptons, and top quarks, which

subsequently decay and produce neutrinos. Higgs bosons can decay into other particles, such as light quarks, but these particles are of little consequence for high-energy neutrino fluxes. Neutrinos from Higgs decay are known as neutrinos from secondary channels since there are two steps in the decay process: a Higgs decays into lighter particles, which in turn decay producing neutrinos. In general, secondary channels do not produce a significant number of high-energy neutrinos because each step in a chain of decays reduces the available energy, but in some regions of parameter space it is possible that they could become important. Usually the Z and W bosons in Higgs-gauge boson channels dominate.

In both the Earth and Sun, the Higgs decay contribution is found by taking the second moment for each decay channel, integrating over a range of energies, and summing over all possible channels. This is written as

$$\langle Nz^2 \rangle_H(E_{\text{in}}) = \frac{1}{E_{\text{in}}^2} \sum_D B_D \frac{1}{2\gamma_H E_f \beta_f \beta_H} \int_{\gamma_H E_f (1-\beta_H \beta_f)}^{\gamma_H E_f (1+\beta_H \beta_f)} E^2 \langle Nz^2 \rangle_f(E) dE. \quad (35)$$

where the sum D is over all possible Higgs decay channels, B_D is the branching ratio for channel D , γ_H is the Lorentz factor for the Higgs, E_f is the decay particle energy in the rest frame of the Higgs, and β_f and β_H are the velocities of the decay particle and the Higgs particle. Equation (35) is used to find the Higgs contribution in Higgs-gauge boson channels, and the second moment for Higgs-Higgs channels.

The branching ratio for H_2^0 decay into up-type fermions is

$$\Gamma(H_2^0 \rightarrow \bar{u}u) = \frac{N_c g^2}{16\pi m_W^2} m_{H_2^0} m_u^2 \left(1 - \frac{4m_u^2}{m_{H_2^0}^2}\right)^{\frac{3}{2}} \frac{\cos^2 \alpha}{\sin^2 \beta} \quad (36)$$

where $N_c = 1$ for leptons and 3 for quarks, due to color, and $g^2 = 8m_W^2 G_F / \sqrt{2}$. The mixing angle α satisfies

$$\tan(2\alpha) = \tan(2\beta) \left(\frac{m_{H_1^0}^2 + m_{H_2^0}^2}{m_{H_3^0}^2 - m_Z^2} \right). \quad (37)$$

For H_2^0 decay into down-type fermions the branching ratio is

$$\Gamma(H_2^0 \rightarrow \bar{d}d) = \frac{N_c g^2}{16\pi m_W^2} m_{H_2^0} m_d^2 \left(1 - \frac{4m_d^2}{m_{H_2^0}^2}\right)^{\frac{1}{2}} \frac{\sin^2 \alpha}{\cos^2 \beta}. \quad (38)$$

The branching ratio for H_3^0 decay is

$$\Gamma(H_3^0 \rightarrow \bar{u}u) = \frac{N_c g^2}{16\pi m_W^2} m_{H_3^0} m_u^2 \left(1 - \frac{4m_u^2}{m_{H_3^0}^2}\right)^{\frac{1}{2}} \frac{\cos^2 \beta}{\sin^2 \beta} \quad (39)$$

for up-type fermions and

$$\Gamma(H_3^0 \rightarrow \bar{d}d) = \frac{N_c g^2}{16\pi m_W^2} m_{H_3^0} m_d^2 \left(1 - \frac{4m_d^2}{m_{H_3^0}^2}\right)^{\frac{1}{2}} \frac{\sin^2 \beta}{\cos^2 \beta} \quad (40)$$

for down-type fermions. The branching ratios for H_1^0 decay are obtained by switching $\cos \alpha$ and $\sin \alpha$ in the equations for H_2^0 decay.

All of the preceding second moments were encoded into `Mathematica`. As a check on the coding, the curves for the second moments given in [68] were reproduced. The required `Neutdriver` information was then read in one model at a time and the event rate from the Sun and Earth for each model determined.

4 Determining Neutralino Properties

4.1 Direct Relationships

Since we are ultimately interested in finding out the nature of the supersymmetric theory that produces a neutralino, an obvious starting point is to study whether there are straightforward relationships between an event rate and the model parameters. Considering the long sequence of steps involved in going from one to the other, it is not surprising that determining model parameters exclusively from an event rate is impossible. For a given value of M_2 , for example, it is possible to construct models with solar event rates ranging from the upper experimental limit ($10^{-2} \text{ m}^{-2}\text{yr}^{-1}$) down to the detection threshold of the next generation of detectors ($10^{-4} \text{ m}^{-2}\text{yr}^{-1}$). Models with event rates well outside this range can be constructed, but are either constrained by experimental results or have event rates too low for detection. Figure 4 shows the relationship between event rates from the Sun and Earth for the values of M_2 explored. The range of event rates for the Earth is greater than for the Sun, extending well below the lower limit of detection, because there are many models that produce a detectable event rate from the Sun when the Earth is unobservable. Since the Sun almost always produces more events than the Earth, there are very few cases where the opposite is true, and the solar events are generally restricted to the $10^{-2} \text{ m}^{-2}\text{yr}^{-1}$ to $10^{-4} \text{ m}^{-2}\text{yr}^{-1}$ range.

The situation is similar for event rates as a function of neutralino properties. Figure 5 shows the event rate from the Sun and Earth versus neutralino mass. As in the case for M_2 , the limits on solar events are a result of the constraints applied, and the terrestrial event rate reaches well below the threshold of detectability because of the models where only the Sun is observed. There is a general trend of decreasing event rate from the Sun, and also to a lesser extent from the Earth, as neutralino mass increases.

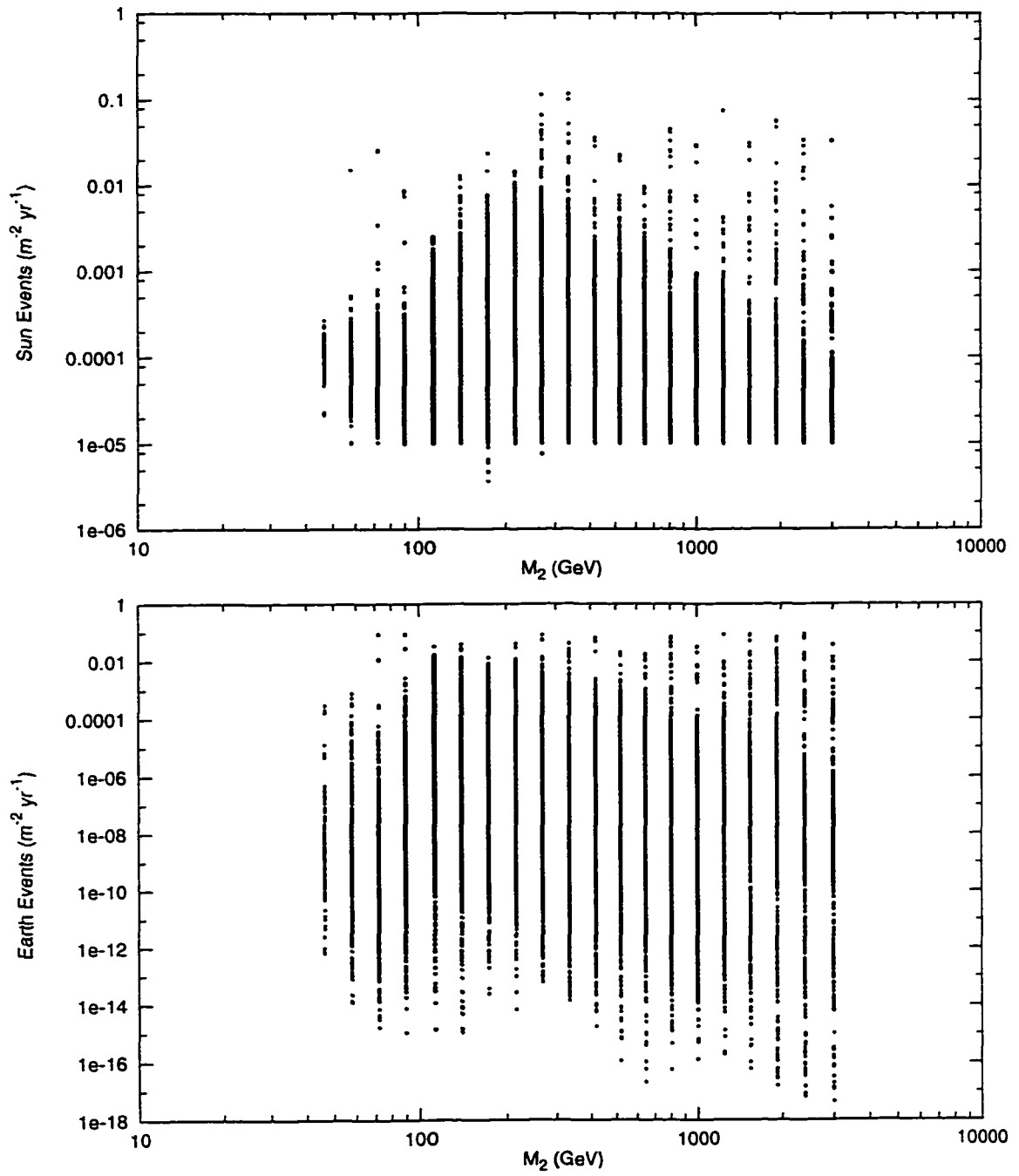


Figure 4: Sun and Earth event rate Γ versus input parameter M_2 .

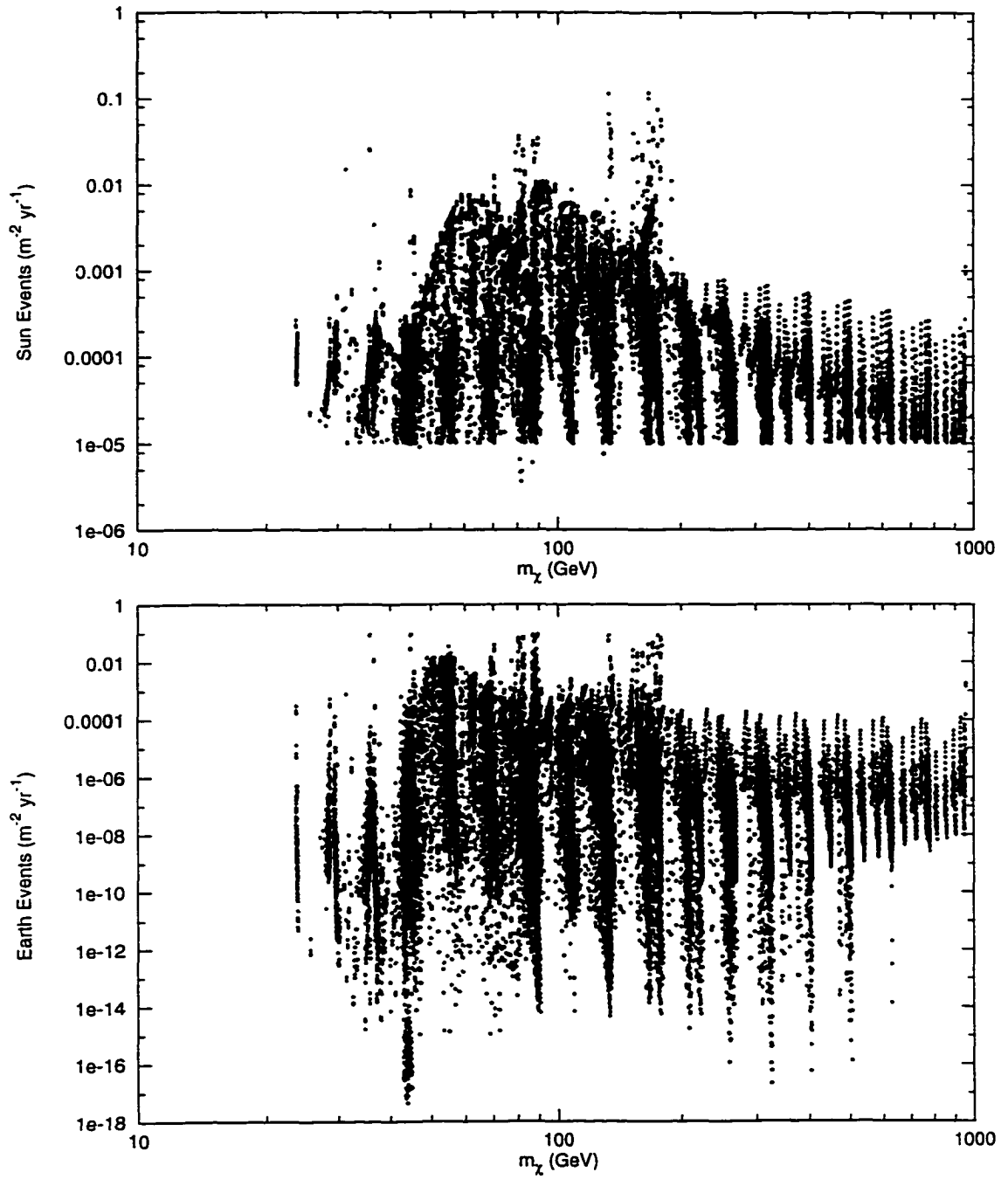


Figure 5: Sun and Earth event rate Γ versus neutralino mass m_χ .

Trends of this kind must be treated with caution. They can result from the way parameter space was sampled and from the indirect influence of the constraints imposed (see section 3.2). A clear example of this is the periodic variation in the density of points in Figure 5, resembling evenly spaced vertical clumps. Each clump approximately represents one value of M_2 in the scan of parameter space. This is obviously not a real effect and it has no physical significance. By choosing different values of M_2 the clumps can easily be shifted back and forth. The slight trend of decreasing event rate with increasing mass, for the values shown in the figure, is not a real effect either. It is possible to produce event rates up to the experimental limit for the Sun and Earth over the entire mass range shown by choosing different input parameters [44]. The scans of parameter space presented here are not exhaustive, but are large enough to illustrate the prospects for determining neutralino properties from indirect event rates.

Similarly, no great meaning should be attached to the density of points in the figures. A greater density of points does not mean models in that region of parameter space are more likely than models in other regions.

Figure 6 shows the event rate as a function of $\Omega_\chi h^2$, the relic universal density of neutralinos. The event rate has a downward trend for both lowest and highest values of $\Omega_\chi h^2$. The decrease for $\Omega_\chi h^2 < 0.025$ is from rescaling the local neutralino density, ρ_χ . These small values of the universal density are no longer consistent with neutralinos making up the entire dark halo of our galaxy. By scaling ρ_χ downward to reflect this, the event rate is reduced. For values of $\Omega_\chi h^2$ approaching the upper limit of 1, the decrease in event rates is related to the annihilation cross section. As depicted in Figure 2, particles with smaller annihilation cross sections freeze out earlier, resulting in a larger relic abundance. The annihilation and elastic scattering cross sections are related, so a smaller annihilation cross section usually indicates smaller elastic cross section, resulting in less neutralino capture and therefore a somewhat lower event

rate.

The gaugino fraction is a useful quantity for describing a neutralino. Equation (6) defines $f_g = 1$ for a neutralino that is purely gaugino, $f_g = 0$ when purely higgsino, and intermediate values represent a mixed state. In general, mixed states have larger scalar (spin-independent) cross sections, while axial-vector (spin-dependent) cross sections are more important in pure states [27]. The Earth captures neutralinos entirely through scalar interactions, but the Sun can also capture neutralinos via axial-vector interactions because of the presence of hydrogen. In Figure 7, a plot of the event rate as a function of gaugino fraction, this is indicated by the Earth event rate reaching its lowest values for pure states.

Although there are some trends in these figures, it is hard to draw any firm conclusions based purely on an event rate. This can be illustrated by choosing a rate and finding the range of parameters that are allowed, within the limits of uncertainty. The three main sources of uncertainty in the calculation are the local halo density, the velocity dispersion of dark matter particles in the halo, and the neutralino scattering cross sections. The largest uncertainty is in the local halo density, with measurements ranging from half to twice the value used, $\rho_\chi = 0.3 \text{ GeV cm}^{-3}$ [18]. Estimates of the velocity dispersion of dark matter particles are more certain, typically ranging from 240 to 330 km s^{-1} [69]. Both these quantities enter into the rate calculation linearly.

The uncertainty in the axial-vector and scalar components of the elastic scattering cross section is harder to quantify. For some direct detection experiments based on axial-vector interactions, the largest source of uncertainty is in the axial-vector cross section, specifically in determining the spin structure of the nucleon. However, this is not as much of a concern for indirect detection of high-energy neutrinos from the Sun [70]. The scalar cross section is perhaps most affected by uncertainties in the pion-nucleon scattering sigma term [27]. Since the uncertainty in the halo density is so large, only it will be used to define the range of uncertainty in the event rate.

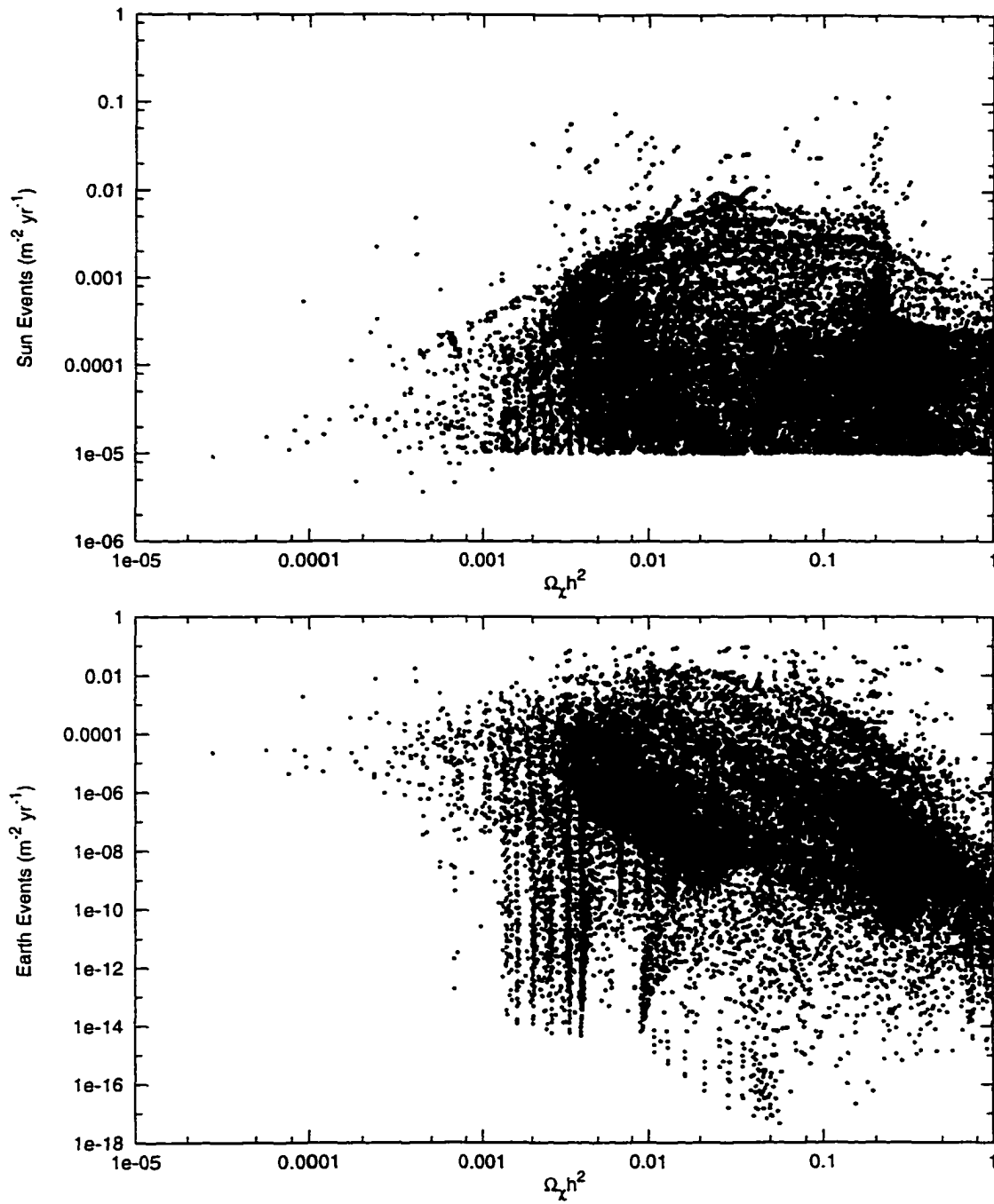


Figure 6: Sun and Earth event rate Γ versus $\Omega_\chi h^2$.

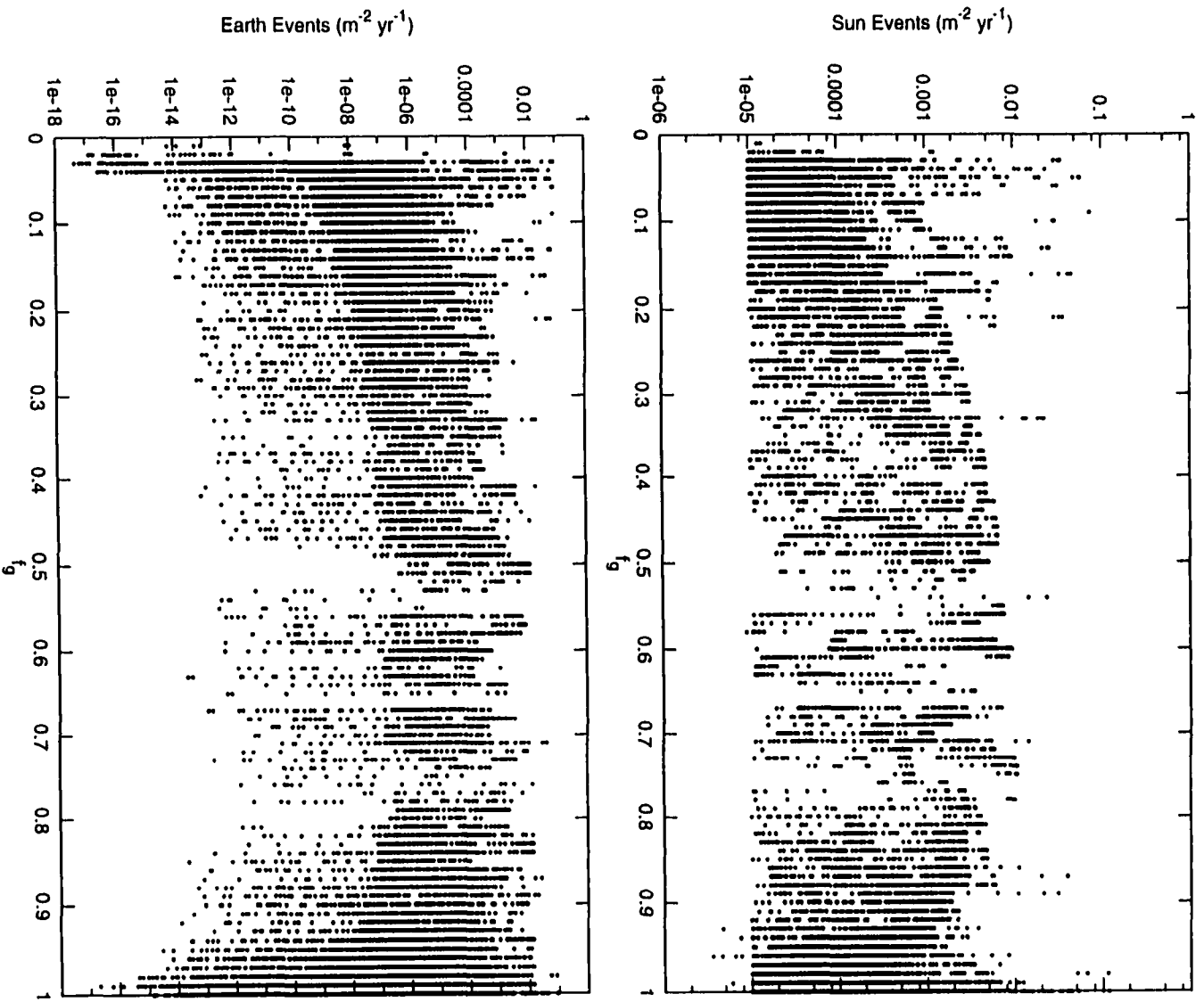


Figure 7: Sun and Earth event rate Γ versus gaugino fraction f_g .

This will not alter the conclusions drawn when examining the allowed parameters for a given event rate, but will simplify the discussion. The result is an underestimate of the total uncertainty and a reduction in the number of models that are compatible with an event rate.

In spite of this, Figure 8 reveals that for the three solar event rates chosen, the entire range of input parameters and neutralino properties is, in most cases, possible. The three event rates are in this respect virtually indistinguishable. There are some differences in the neutralino mass, where the upper limit increases as the event rate decreases. This is the same effect discussed earlier in the figure of m_χ versus event rate (Figure 5), which can be attributed to how parameter space was sampled. It is evident that deriving neutralino properties or supersymmetric model parameters entirely from an event rate is unlikely.

4.2 Sun-Earth Event Ratio

A way of potentially getting more information from event rates is examining the Sun-Earth event ratio $\Gamma_\odot/\Gamma_\oplus$ and relating differences in the ratio back to the neutralino properties that cause the deviation [63, 66]. The two main reasons for variations in the event ratio are differences in how the Sun and Earth capture neutralinos, and whether or not the Earth has had enough time for capture and annihilation to reach equilibrium.

4.2.1 Neutralino Capture

The scattering of neutralinos takes place in the extreme non-relativistic limit. As mentioned previously, only two kinds of interactions are important in this situation: axial-vector (spin-dependent) and scalar (spin-independent). In the first case, the neutralino couples to the spin of a nucleus; in the second it couples to the mass. At

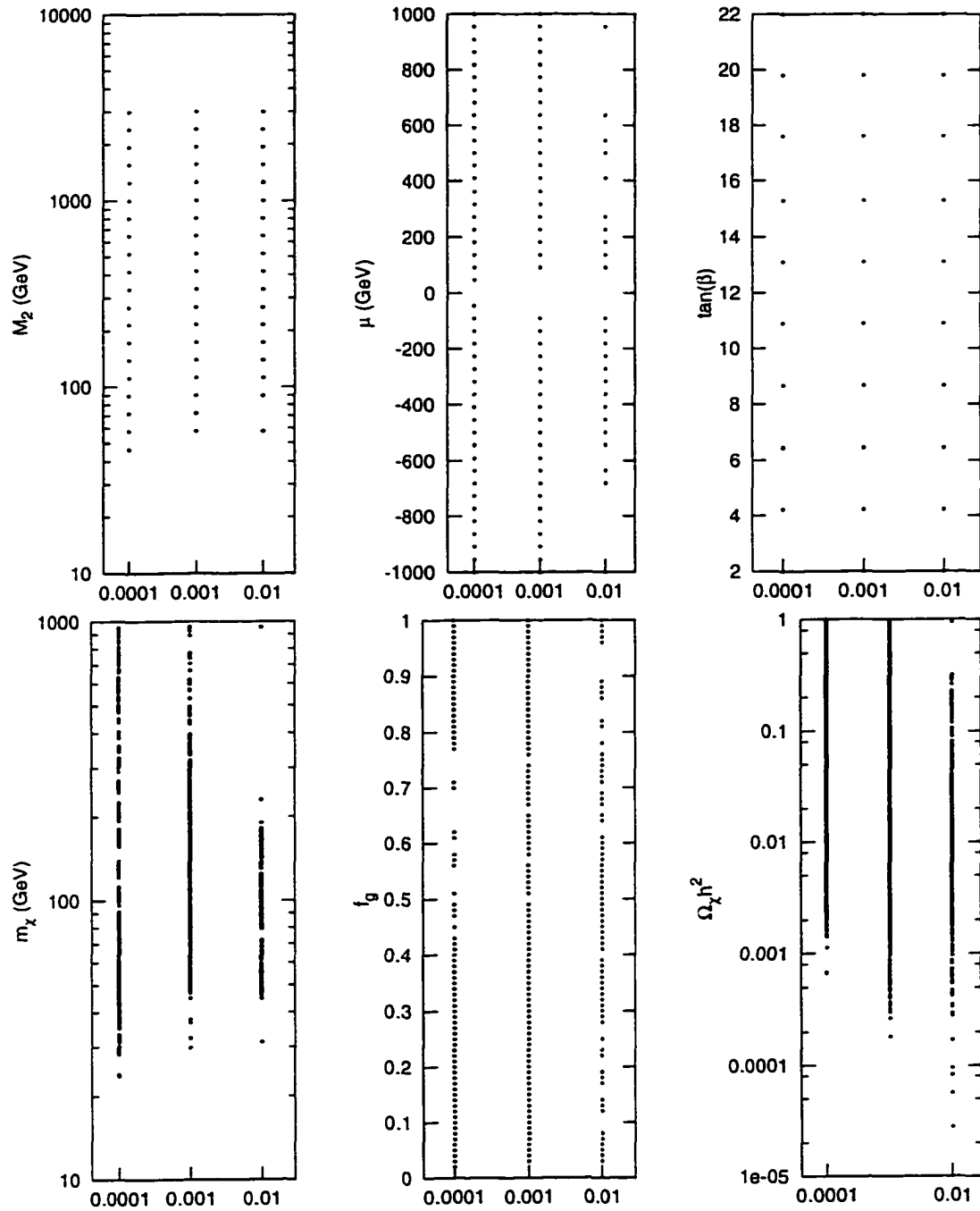


Figure 8: Comparison of three solar event rates for different input parameters and neutralino properties. The rates chosen are 10^{-2} , 10^{-3} , and $10^{-4} \text{ m}^{-2} \text{ yr}^{-1}$, with a factor of two uncertainty.

first it was thought that only the Sun would have a capture rate large enough to produce a detectable neutrino flux. Neutralino energies follow a Maxwell-Boltzmann distribution with a velocity dispersion of $\bar{v} = 270 \text{ km s}^{-1}$ [27]. The escape velocity at the surface of the Sun is 618 km s^{-1} , but merely 11.2 km s^{-1} at the surface of the Earth [61]. Only the few neutralinos on the low energy tail of the distribution have a chance of being captured by the Earth.

As Gould later pointed out, there can be a resonance enhancement of neutralino capture in the Earth [61]. If the neutralino undergoes scalar interactions and the mass of the neutralino matches the mass of the nucleus it scatters from, there is a greater chance it will be captured. The explanation for this is analogous to the classical case of an elastic collision between two bodies. If they are equal in mass, the incoming body transfers most its energy to the target in a head-on collision, coming to rest and becoming captured. If the target is massive, the incoming body recoils with essentially the same speed; if the target is relatively small, it has little effect on the incoming body and it maintains the same velocity. In both these cases, there is little chance for a reduction in speed to less than v_{escape} . For neutralino masses near those of ^{16}O , ^{24}Mg , ^{28}Si , ^{32}S , ^{40}Ca , ^{56}Fe , or ^{58}Ni the capture rate is greatly enhanced. Virtually the entire neutralino mass range from 10 to 90 GeV is near one of these resonances. There is no such enhancement in the Sun: the escape velocity is so large compared to the Earth's that neutralinos with a wide range of masses are already captured relatively easily.

There are cases where the momentum transfer is large and the neutralino does not "see" the entire nucleus, reducing the scalar cross section. This is analogous to the effect seen in electromagnetic elastic scattering of electrons from atoms and nuclei. In the Earth, form factor suppression is greatest in the same mass range where resonance is greatest, the 10 to 80 GeV range. However, the overall effect on Earth capture rates is small for light neutralinos and negligible for heavier neutralinos. In the Sun, where

the gravitational well is deeper and neutralinos undergo higher momentum transfer when scattering, the effect is more important. There is a small to moderate effect on light elements, but capture from iron nuclei can be reduced by several orders of magnitude. Overall solar capture rates can be reduced by as much as 30% for an 80 GeV neutralino [27].

The differences between scalar capture in the Sun and Earth are apparent in Figure 9, a plot of the event ratio as a function of neutralino mass. The Sun-Earth ratio $\Gamma_{\odot}/\Gamma_{\oplus}$ reaches its smallest value for neutralino masses of 50-60 GeV, about the same mass as iron (52 GeV). Resonance with iron in the Earth increases the Earth capture rate relative to the Sun, increasing the number of muon events from the Earth and lowering the event ratio. At the same time, form factor suppression in the Sun lowers the solar capture and event rate, pushing the event ratio even lower. The models generated indicate that if solar events are 0.1 to 0.01 that of terrestrial events, the neutralino mass will be near that of iron. As the ratio approaches one, the range of possible masses widens quickly to the point where no conclusions can be drawn.

The other type of interaction is axial-vector (spin-dependent), where the neutralino couples to the spin of the atom. Of all the abundant elements in the Sun and Earth, only hydrogen in the Sun couples to neutralinos through axial-vector interactions. If neutralinos undergo only this type of interaction, there will be no capture in the Earth. At first this was thought to be the case, but Griest [71] discovered that neutralinos that are mixed states can also have scalar couplings, making capture by the Earth possible.

The existence of axial-vector capture in the Sun but not in the Earth alters the event ratio by increasing the solar event rate in models where neutralinos have axial-vector couplings, so the ratio $\Gamma_{\odot}/\Gamma_{\oplus}$ increases. Pure states, indicated by a gaugino fraction f_g of 0 or 1, are more likely to have stronger axial-vector couplings. This

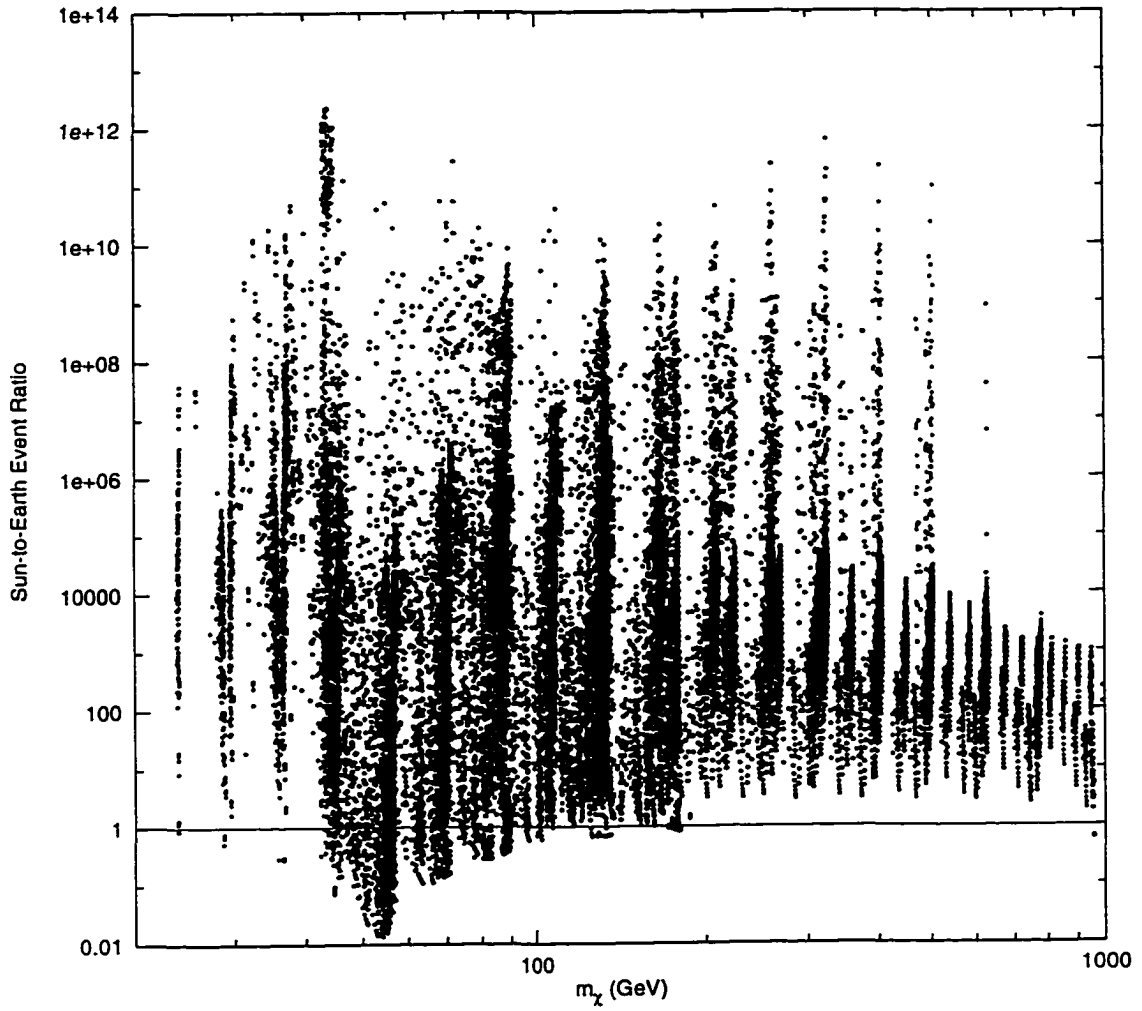


Figure 9: Event ratio $\Gamma_{\odot}/\Gamma_{\oplus}$ versus neutralino mass m_{χ} . Note the existence of events with a ratio less than 1 between $m_{\chi} \sim 30 - 100$ GeV.

is visible in Figure 10, where the largest event ratio occurs for these values of f_g . Because the top quark is heavy, even pure states may have scalar interactions [27]. This is the case in the models generated, since there are no models where the Earth event rate is zero.

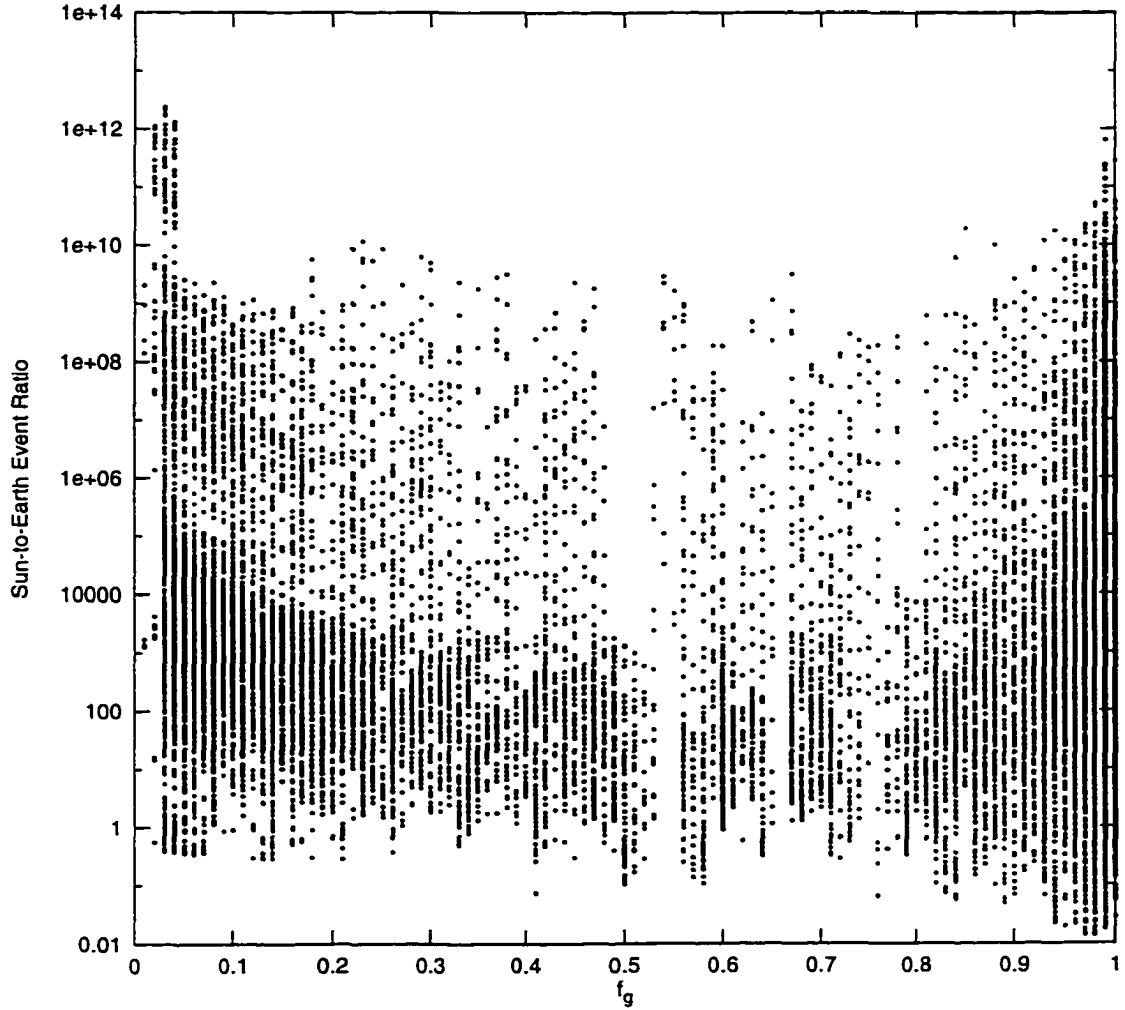


Figure 10: Event ratio $\Gamma_{\odot}/\Gamma_{\oplus}$ versus gaugino fraction f_g .

4.2.2 Equilibrium Time Scale

The other reason there may be a large variation in the Sun-Earth event ratio is because of the equilibrium time scale. After the Sun and Earth formed approximately 4.5 Gyr

ago it took time for neutralinos to accumulate. The capture rate remains constant, but until enough neutralinos have accumulated, the annihilation rate is less than its maximum value of $\Gamma_A = C/2$. There are not enough neutralinos interacting with each other for annihilation to occur as quickly as capture. The number of neutralinos eventually builds up to a point where capture and annihilation balance and the body is at “full signal.” The amount of time this takes is called the equilibrium time scale. The Sun is more massive and captures neutralinos relatively quickly, so it always reaches full signal before the Earth [61]. In virtually every case where the Sun is observable, it is at full signal. The Earth, however, can often be below full signal.

Gould [63] suggested this difference between the Earth and Sun could be used to constrain or estimate the relic universal density of neutralinos, $\Omega_\chi h^2$. This is done by relating how far the Earth is from full signal to the neutralino’s annihilation cross section. A smaller cross section means more neutralinos must accumulate before capture and annihilation balance. If the cross section is larger, fewer neutralinos are needed and the equilibrium time scale is shorter. Since the annihilation cross section also determines the relic abundance of neutralinos, an estimate of the cross section leads to an estimate of the relic abundance. Using the supersymmetric models generated, it is possible to check the usefulness of this approach for a wide range of possible neutralinos.

The relationship between the thermally averaged neutralino annihilation cross section and the relic density is [1]

$$\Omega_\chi h^2 \sim \frac{3 \times 10^{-27} \text{ cm}^3 \text{ s}^{-1}}{\langle \sigma_A v \rangle} \left(\frac{g_f}{88} \right)^{-1/2} \frac{m_\chi c^2}{25kT_f} \quad (41)$$

where g_f is the number of relativistic degrees of freedom at freezeout and T_f is the freezeout temperature. Using typical weak scale numbers, the freezeout temperature is approximately $T_f \simeq m_\chi/20$ and $g_f/88 \simeq 1$ [27]. Putting these values into equation

(41). the relic density is

$$\Omega_\chi h^2 \sim \frac{2 \times 10^{-27} \text{ cm}^3 \text{ s}^{-1}}{\langle \sigma_A v \rangle}. \quad (42)$$

To estimate the relic density, an estimate of the annihilation cross section is needed. Recall that the annihilation rate is related to the capture rate by equation (12)

$$\Gamma_A = \frac{C}{2} \tanh^2 \left(\frac{t}{\tau} \right).$$

The ratio t/τ determines whether the Sun or Earth is at full signal. When the equilibrium time scale, τ , is much smaller than t , the age of the solar system, the formula reduces to the full signal case of $\Gamma_A = C/2$. For the Earth, using $t = 4.5$ Gyr. t/τ is [27]

$$\frac{t}{\tau_\oplus} = 2.0 \times 10^4 \left(\frac{C_\oplus}{\text{sec}^{-1}} \right)^{1/2} \left(\frac{\langle \sigma_A v \rangle_0}{\text{cm}^3 \text{ sec}^{-1}} \right)^{1/2} \left(\frac{m_\chi}{10 \text{ GeV}} \right)^{3/4}. \quad (43)$$

The annihilation cross section given here, $\langle \sigma_A v \rangle_0$, is the zero velocity cross section because neutralino annihilation in the Sun and Earth occurs at essentially the zero velocity limit. The annihilation cross section at freezeout, $\langle \sigma_A v \rangle$, when temperatures and velocities are higher, may be larger. The factor

$$\kappa \equiv \frac{\langle \sigma_A v \rangle_0}{\langle \sigma_A v \rangle} \quad (44)$$

relates the cross section for neutralino annihilation in the Sun and Earth back to the cross section that determines the relic abundance at freezeout.

Following the procedure used by Gould [63], there are three cases to consider. In the first, the Sun and Earth have muon event rates that are similar. Assuming this is because the Earth is at full signal, then from equation (12) we know $t/\tau_\oplus \gtrsim 1$. Using this relationship and equation (43), solving for the annihilation cross section gives

$$\langle \sigma_A v \rangle_0 \gtrsim 4.3 \times 10^{-26} \text{ cm}^3 \text{ sec}^{-1} \gamma \left(\frac{C_\oplus}{10^{24} \text{ sec}^{-1}} \right)^{-1} \left(\frac{m_\chi}{100 \text{ GeV}} \right)^{-3/2} \quad (45)$$

where γ is the ratio of capture rates in the Sun and Earth. The squares of their respective distances are scaled out so

$$\gamma \equiv \frac{C_{\odot}/(1 \text{ a.u.})^2}{C_{\oplus}/R_{\oplus}^2} = 1.82 \times 10^{-9} \frac{C_{\odot}}{C_{\oplus}}.$$

Combining equation (45) and equation (42), and using κ to relate the freezeout cross section to the zero velocity cross section, an upper limit of [63]

$$\Omega_{\chi} h^2 \lesssim 0.05 \kappa \gamma^{-1} \left(\frac{C_{\odot}}{10^{24} \text{ sec}^{-1}} \right) \left(\frac{m_{\chi}}{100 \text{ GeV}} \right)^{3/2} \quad (46)$$

is placed on the relic density of neutralinos. (Note that in [63], the constant at the front of the relic density estimate equations (4.4) (4.5) and (4.6) is incorrect).

As noted in [63], the difficulty with this estimate is that it requires knowing the neutralino's mass, the relationship between the zero velocity annihilation cross section and the cross section at freezeout, the ratio of capture rates in the Sun and Earth, and the capture rate in the Sun. Setting aside these difficulties for the moment, the relic density estimate can be demonstrated using model information provided by *Neutdriver*. Most of the information required is available, but the ratio κ of annihilation cross sections needs to be estimated. The annihilation cross section can be written in the form

$$\langle \sigma_{\mathcal{A}} v \rangle = a + bv^2 + \dots \quad (47)$$

The a and b terms are available in output from the supersymmetric models. In the extreme non-relativistic limit for annihilations in the Sun and Earth, the cross section $\langle \sigma_{\mathcal{A}} v \rangle_0$ is simply the a term. For the velocity at freezeout, the freezeout temperature is used to determine particle velocities. Using the approximation $T_f \simeq m_{\chi}/20$, the mean velocity of particles in a Maxwell-Boltzman distribution is

$$v_m = \sqrt{\frac{2kT}{m_{\chi}}} = \sqrt{\frac{c^2}{10}} \simeq 0.3c \quad (48)$$

at freezeout. Using this velocity and the b term in equation (47) gives the freezeout annihilation cross section $\langle \sigma_{\mathcal{A}} v \rangle$ and κ .

With this information the relic density limit can be tested. In the density estimates, the Earth is considered to be at full signal when $t/\tau_{\oplus} > 1$, so that $2\Gamma_{A\oplus}/C_{\oplus} > 0.58$. Figure 11 shows the estimated upper limit on the relic density is always nearly equal to or greater than the relic density calculated for each model by **Neutdriver**. Of course, the estimate is somewhat artificial since the information needed (capture rates, neutralino mass, cross sections) is provided by **Neutdriver**, but it does indicate the potential of this approach.

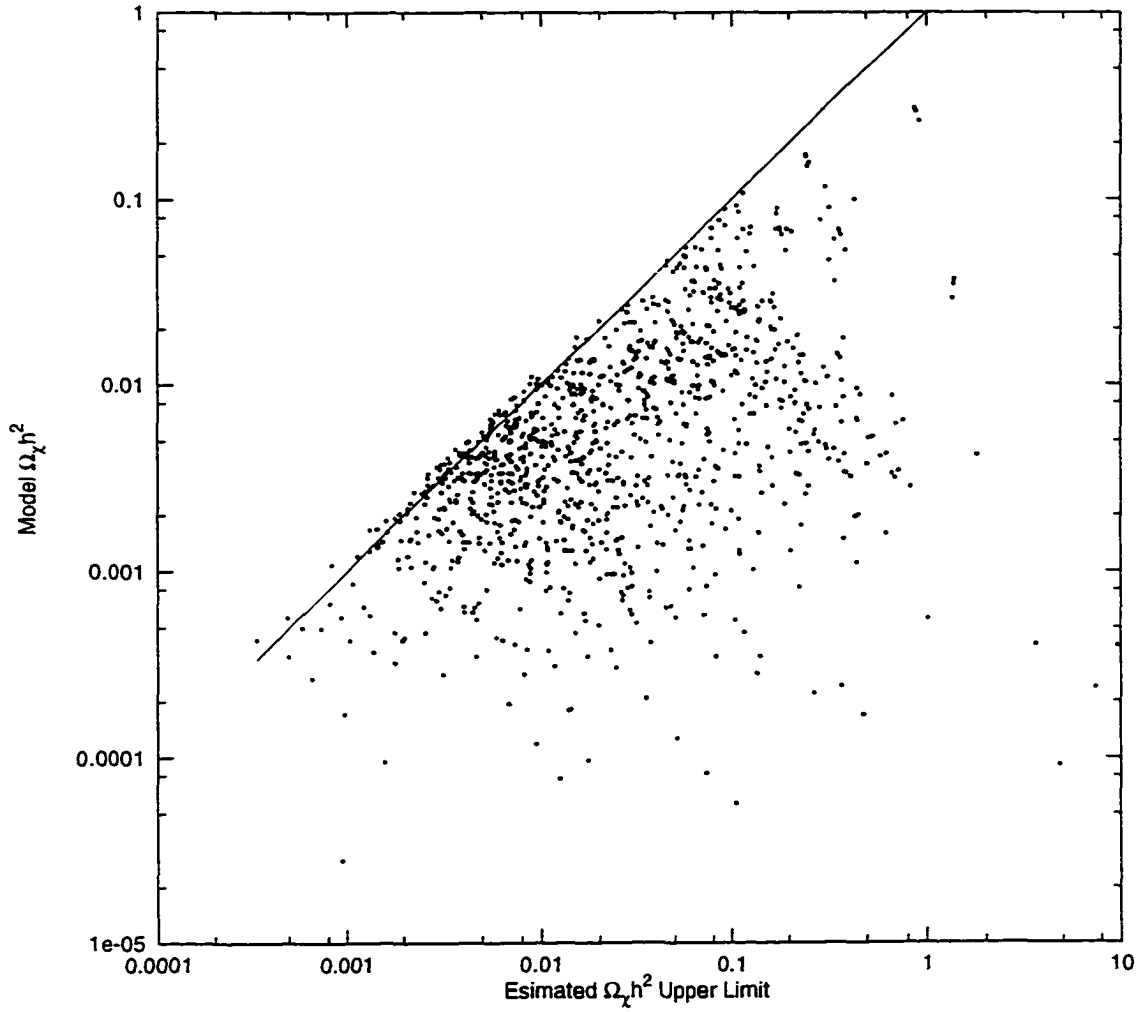


Figure 11: $\Omega_{\chi} h^2$ generated in the supersymmetric model versus the estimated upper limit on $\Omega_{\chi} h^2$. The solid line marks when the two are equal.

In the second scenario considered, the Sun and Earth are both detected but the signal from the Earth is small compared to the Sun. Assuming this is because the Earth has not yet reached full signal, an estimate of the relic density can be made. When the Earth is below full signal, the equilibrium time scale is longer than the age of the solar system and $2\Gamma_{A\oplus}/C_{\oplus} < 1$. Using equation (12),

$$\frac{2\Gamma_{A\oplus}}{C_{\oplus}} = \tanh^2\left(\frac{t}{\tau_{\oplus}}\right) \simeq \left(\frac{t}{\tau_{\oplus}}\right)^2. \quad (49)$$

Following the same procedure as above when the Sun and Earth rates were comparable gives an estimate of the relic density [63]

$$\Omega_{\chi} h^2 \sim 0.05 \kappa \gamma^{-1} \frac{C_{\oplus}}{2\Gamma_{A\oplus}} \left(\frac{C_{\odot}}{10^{24} \text{ sec}^{-1}}\right) \left(\frac{m_{\chi}}{100 \text{ GeV}}\right)^{3/2}. \quad (50)$$

The results are shown in Figure 12. Once again, there is good agreement between the estimate and the model calculation.

Finally, in cases where the Sun is detected but the Earth is not, a lower bound can be placed on the relic density. If the Earth is undetectable, its annihilation rate must be below the minimum required for producing a detectable signal above $\Gamma_{\oplus} \sim 10^{-5} \text{ m}^{-2}\text{yr}^{-1}$ events. Figure 13 demonstrates that the event rate $\Gamma_{\oplus} \propto \Gamma_{A\oplus} m_{\chi}^2$. The cut-off for Earth detection occurs around $\Gamma_{A\oplus} m_{\chi}^2 \sim 2 \times 10^{16}$. Adopting this value in equation (50) gives a lower limit on the relic density of

$$\Omega_{\chi} h^2 \gtrsim 0.05 \kappa \gamma^{-1} \frac{C_{\oplus}}{2} \left(\frac{m_{\chi}^2}{2 \times 10^{16}}\right) \left(\frac{C_{\odot}}{10^{24} \text{ sec}^{-1}}\right) \left(\frac{m_{\chi}}{100 \text{ GeV}}\right)^{3/2}. \quad (51)$$

These models are shown in Figure 14. Most of the models generated fall into this category. The estimated lower limit can extend down to extremely small values of $\Omega_{\chi} h^2$. to the point of being a somewhat useless constraint.

4.3 Practical Application of the Neutralino Density Estimate

The previous section demonstrates that it is possible in principle to estimate the relic density of neutralinos in the universe based on the Sun-to-Earth event ratio.

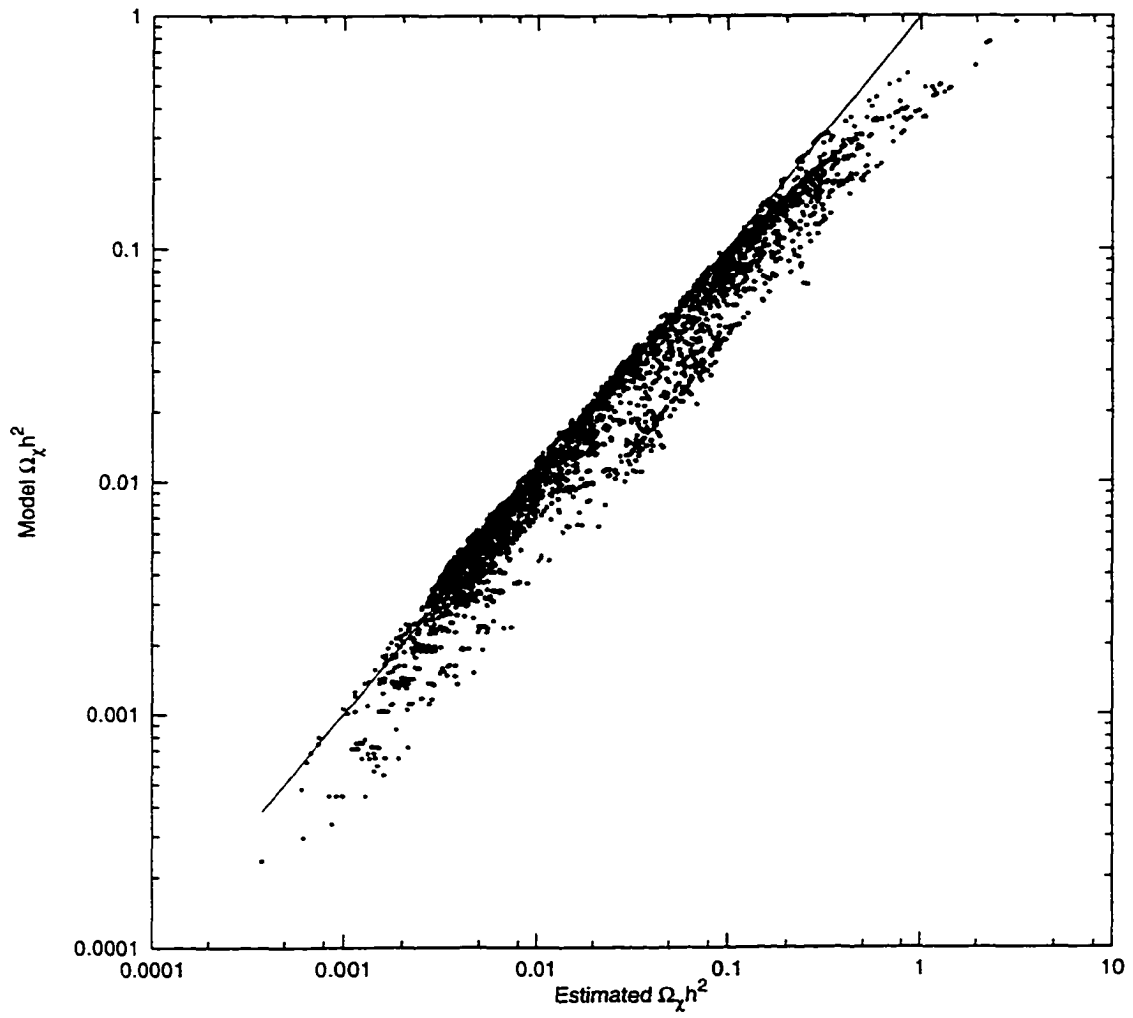


Figure 12: $\Omega_\chi h^2$ generated in the supersymmetric model versus the estimated $\Omega_\chi h^2$. The solid line marks when the two are equal.

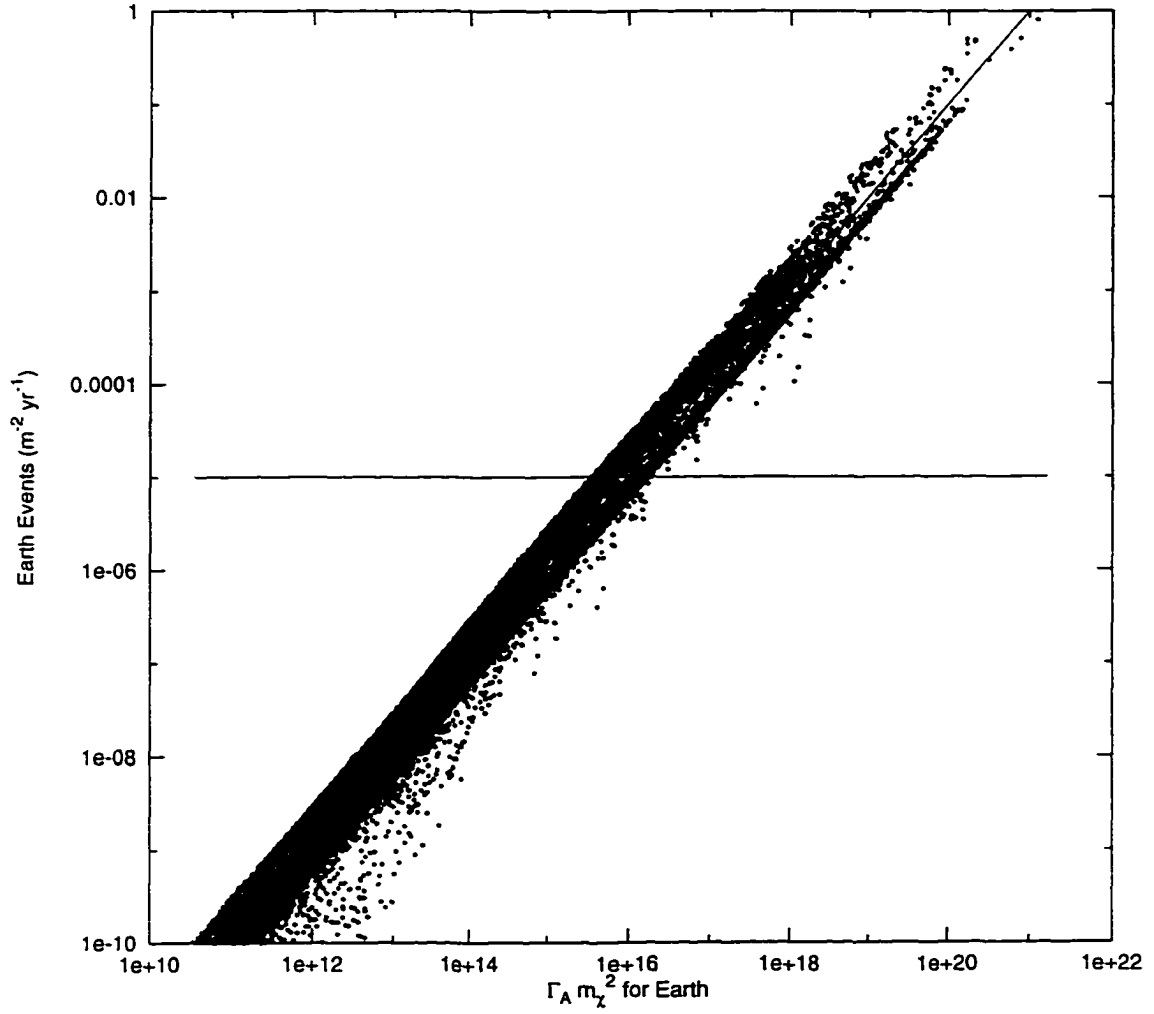


Figure 13: Earth event rate Γ_{\oplus} versus $\Gamma_{A\oplus} m_{\chi}^2$. The cut-off event rate for indirect detection of the Earth is indicated by the horizontal line at 10^{-5} . The line through the data is $10^{-21} \Gamma_{A\oplus} m_{\chi}^2$.

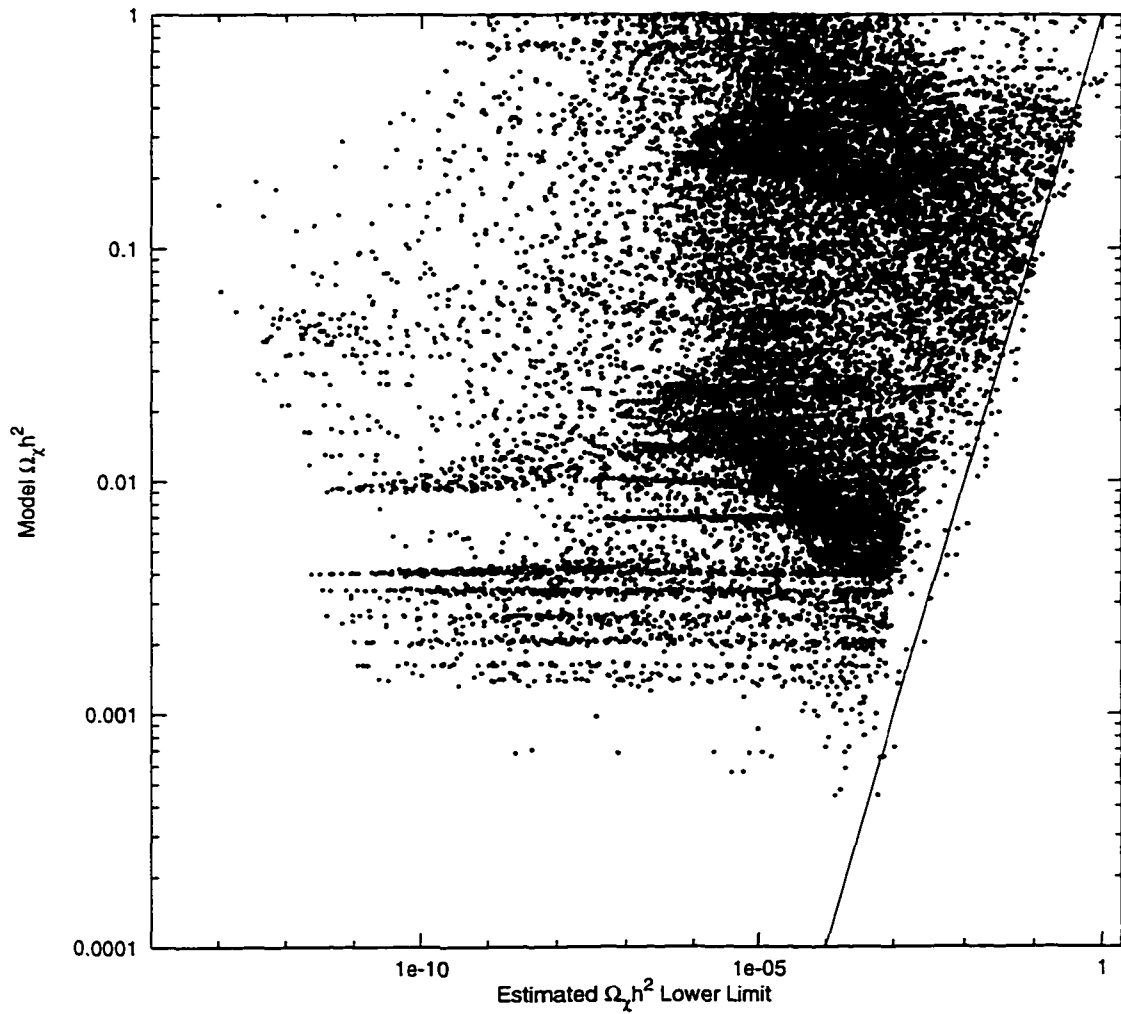


Figure 14: $\Omega_\chi h^2$ generated in the supersymmetric model versus the estimated lower limit on $\Omega_\chi h^2$. The solid line marks when the two are equal.

In practice, there are some difficulties that must be overcome. Actually making an estimate of $\Omega_\chi h^2$ requires several pieces of information either in addition to or derived from the event rates. The neutralino mass, the relationship between the zero velocity annihilation cross section and the cross section at freezeout, and the capture rates for the Sun and Earth are required in the density estimate.

4.3.1 Neutralino Mass and Annihilation Cross Section Ratio

The neutralino mass may be found using other methods. Extracting information about the neutralino mass from the angular distribution of high-energy neutrinos is one possibility. Detectors that use Čerenkov light can track the path of muon events and measure the size of the source. If neutralinos are heavy, they will reside nearer to the centre of the Sun or Earth, resulting in a smaller angular distribution. Lighter neutralinos will be more diffuse, resulting in a wider angular distribution. Both the Sun and Earth could yield a rough mass estimate for neutralinos below 300 GeV with an uncertainty of a factor of 1.5. Detector resolution limits result in heavier neutralinos appearing as a point source [72].

Information about κ , as well as neutralino mass, could eventually come from accelerator searches. The size of the uncertainty introduced by not knowing κ can be quite large. In the models created, κ can range downward several orders of magnitude from its maximum value of 1 when neutralino masses are below about 100 GeV. Above 100 GeV, values tend to stay in the 0.1 to 1 range (Figure 15). An order of magnitude uncertainty in κ results in an order of magnitude uncertainty in the relic density estimate.

4.3.2 Relating Event, Capture, and Annihilation Rates

The density estimate requires deriving the solar and terrestrial capture rates from their event rates. This is accomplished in two steps. First, the neutralino annihilation

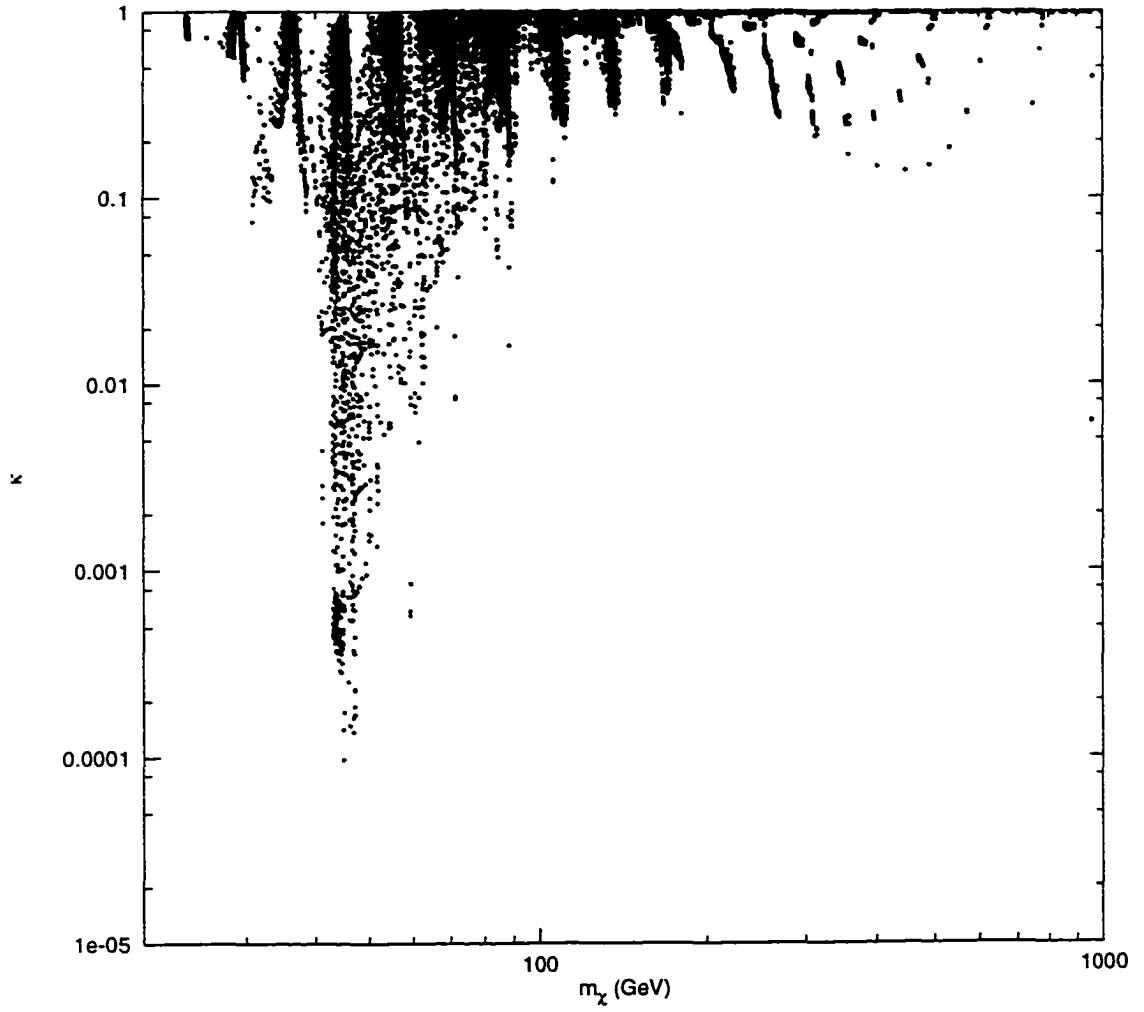


Figure 15: $\kappa \equiv \frac{\langle \sigma_{Av} \rangle_0}{\langle \sigma_{Av} \rangle}$ versus neutralino mass m_χ .

rate within the Sun is estimated using the event rate from the Sun. Since the Sun is always at full signal, the capture rate is simply the twice the annihilation rate. Then, the Earth's capture rate is calculated based on the Sun's. The analysis in [63] finds the Sun-to-Earth capture ratio γ will range from roughly 1 to 6.5 for neutralinos with masses of 80 GeV to 1000 GeV, assuming they are captured predominately by scalar interactions. Comparing the annihilation rate within the Earth (found using its measured event rate in an indirect detector) to its calculated capture rate reveals whether or not the Earth is at full signal, allowing a density estimate.

The primary difficulty is that there is no simple relationship between the event rate from the Sun and the annihilation rate within the Sun. Figure 13 showed that in the Earth, where a lower density means neutralino annihilation byproducts and escaping neutrinos undergo few interactions, the relationship between the annihilation and event rate is relatively well behaved. But in the Sun, the dense solar medium makes relating the annihilation and event rate to any degree of accuracy nearly impossible (Figure 16). The various particles involved in decay chains that produce neutrinos are affected to different extents by interactions with the solar medium, as are the neutrinos they produce. This introduces a much greater model dependence. Variations in decay channels, annihilation channels, branching fractions, and other parameters that make a detailed event rate calculation necessary end up blurring the relationship between annihilation and event rate.

Re-calculating the relic density limits, this time using an estimate of neutralino capture that is based on indirect detector event rates (instead of using the capture rates provided by `Neutdriver`), the error introduced by this model dependence becomes apparent. The upper limit is too low as often as not (Figure 17), and the estimate of $\Omega_\chi h^2$ is typically spread over two orders of magnitude (Figure 18). The lower limit is only violated in a small number of models, but the constraint it applies to $\Omega_\chi h^2$ is usually weak (Figure 19).

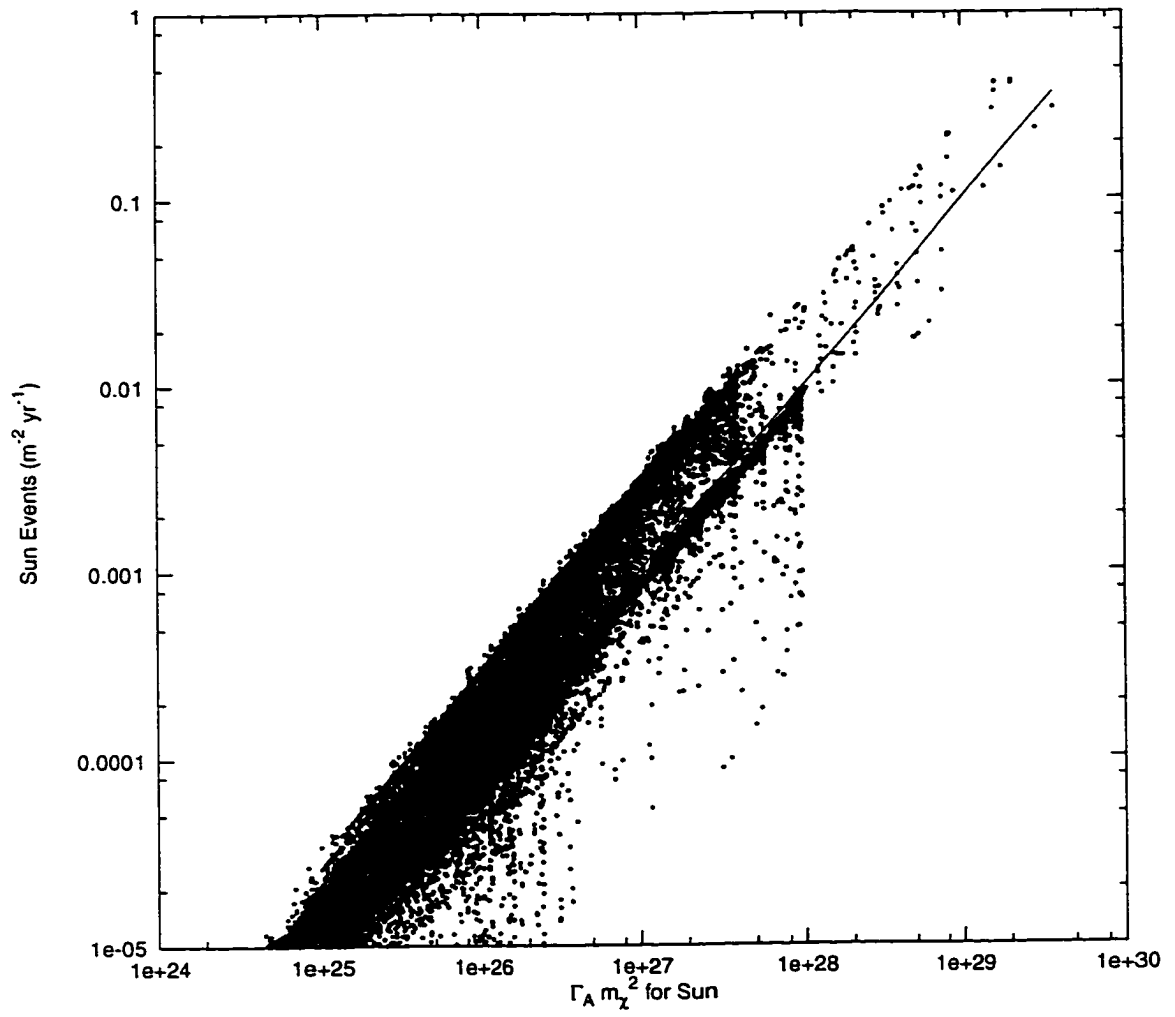


Figure 16: Solar event rate Γ_{\odot} versus $\Gamma_{A\odot} m_{\chi}^2$. The solid line is $10^{-30} \Gamma_{A\odot} m_{\chi}^2$.

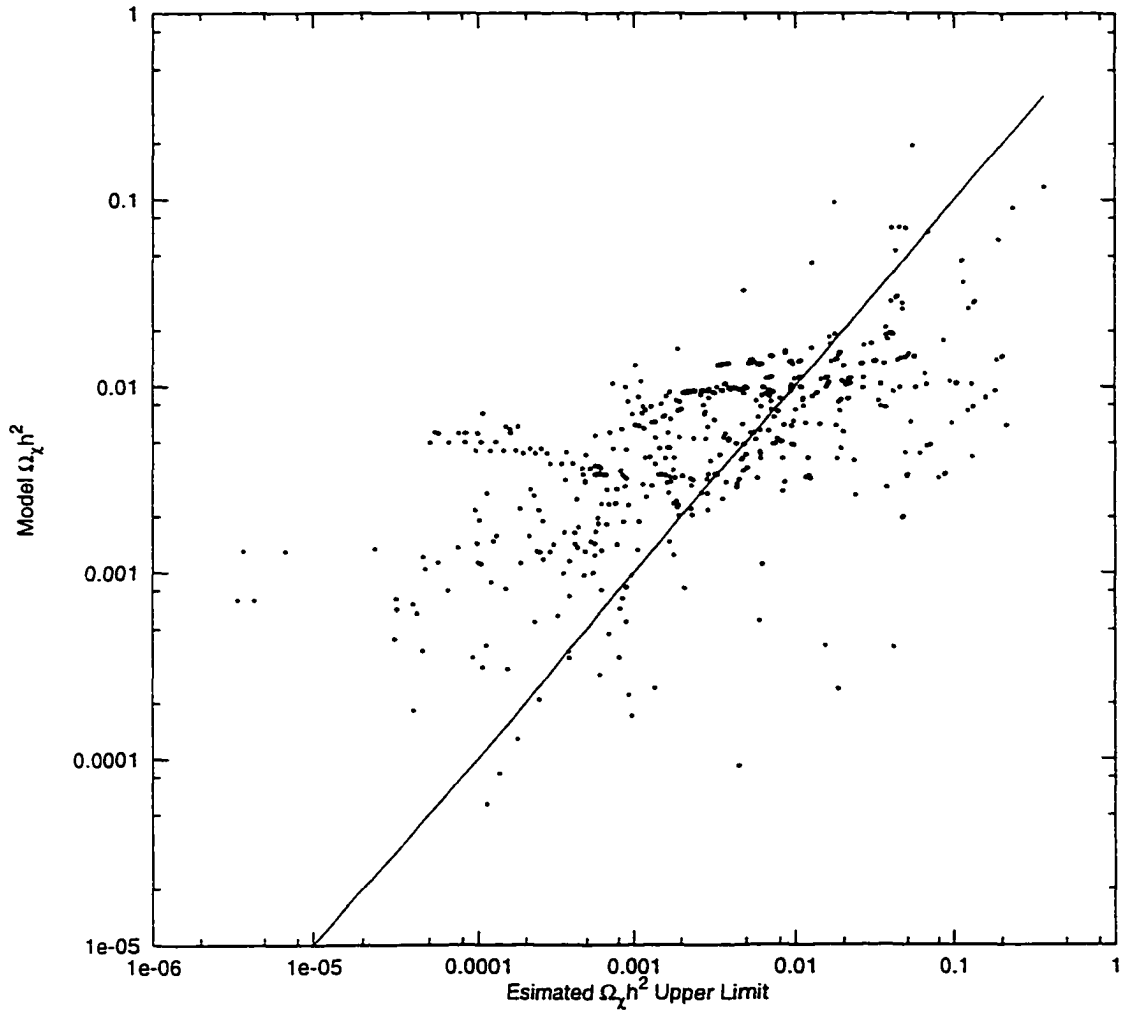


Figure 17: Re-calculation of the estimated upper limit on $\Omega_\chi h^2$ using information derived from event rates. The solid line marks when the two are equal. Only models with $m_\chi > 80$ GeV are used.

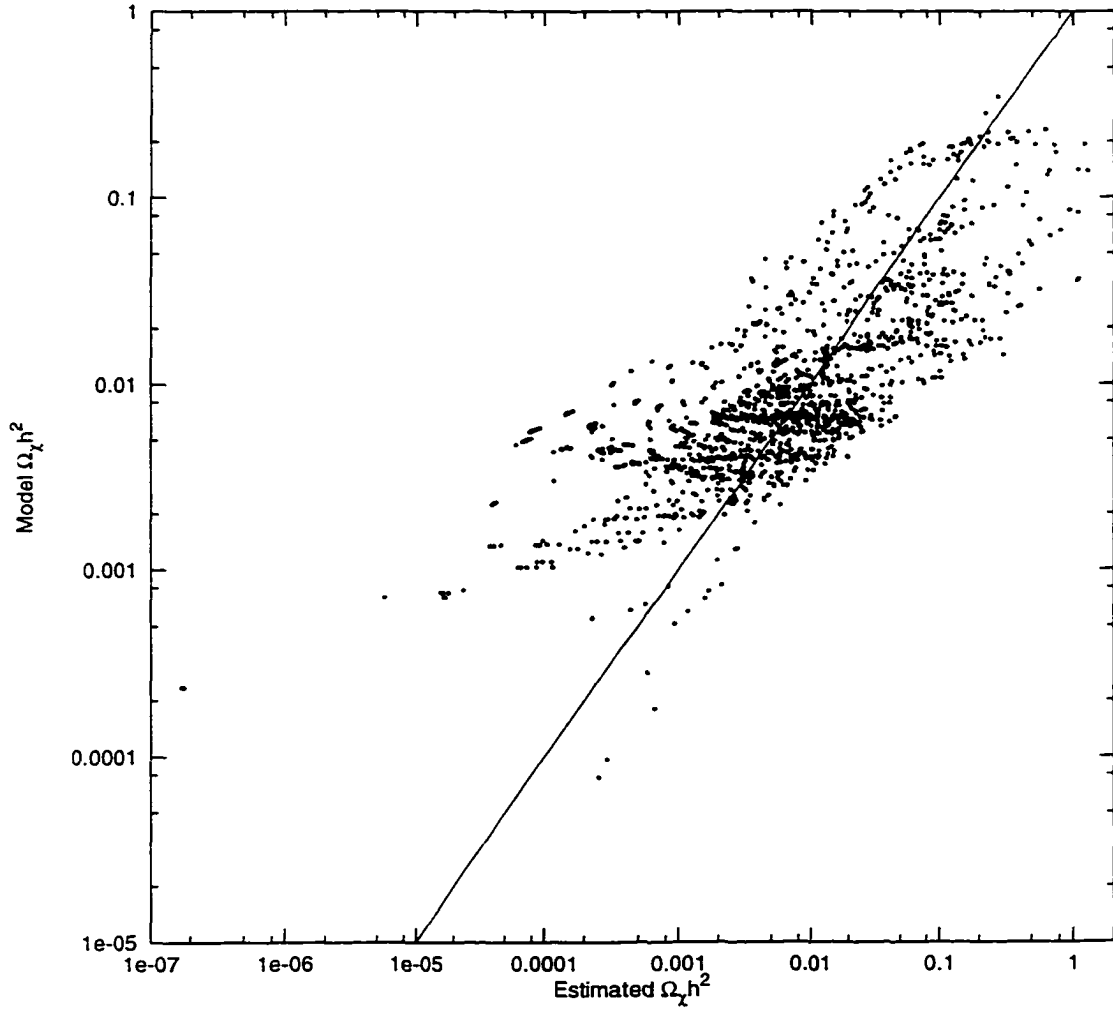


Figure 18: Re-calculation of the estimated $\Omega_\chi h^2$ using information derived from event rates. The solid line marks when the two are equal. Only models with $m_\chi > 80$ GeV are used.

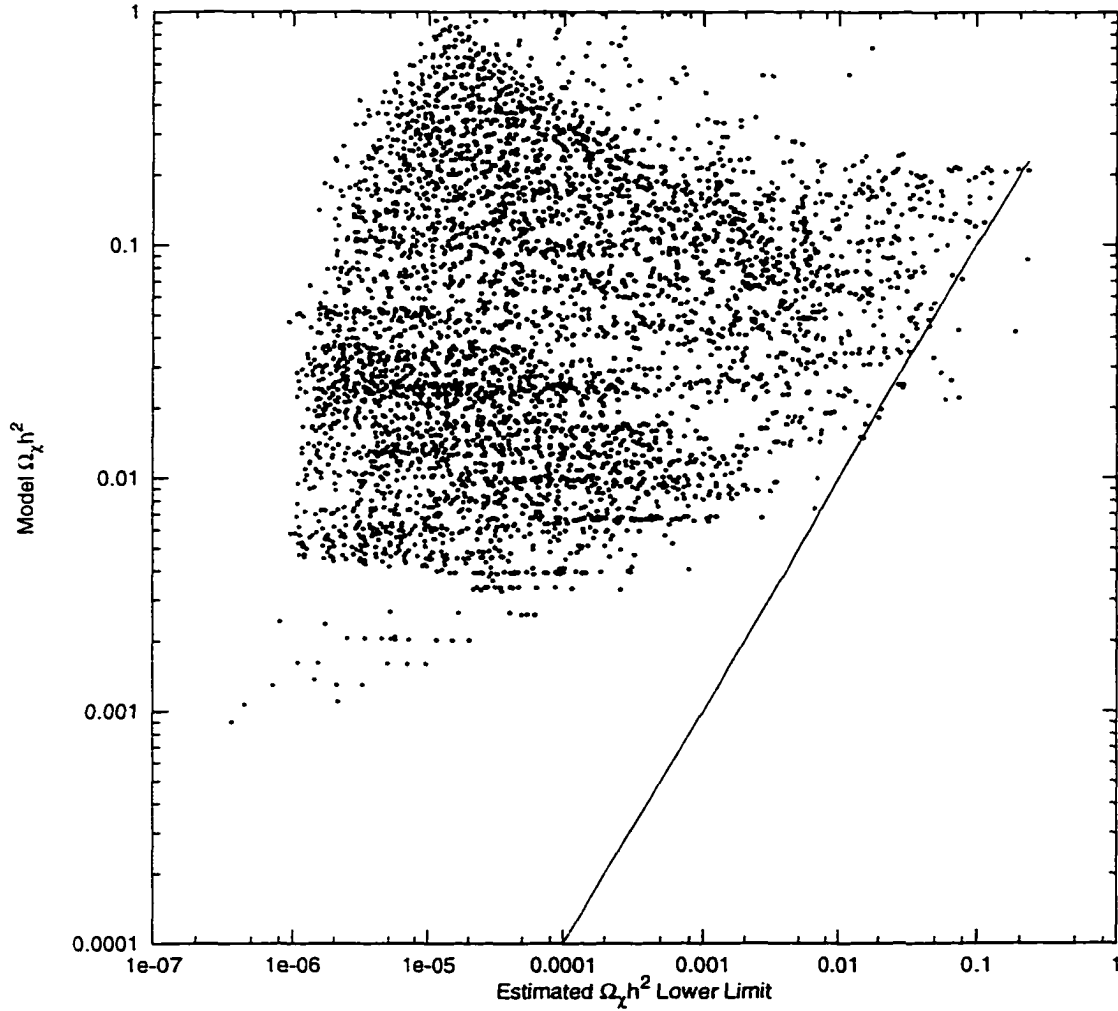


Figure 19: Re-calculation of the estimated lower limit on $\Omega_\chi h^2$ using information derived from event rates. The solid line marks when the two are equal. Only models with $m_\chi > 80$ GeV are used.

For the re-calculation, a simple relationship of $\Gamma_{\odot} = 10^{-30} \Gamma_{A\odot} m_{\chi}^2$ is assumed for the Sun and $\Gamma_{\oplus} = 10^{-21} \Gamma_{A\oplus} m_{\chi}^2$ for the Earth. These relations are about what one would expect based on equation (13), considering the losses from interactions and decay channels that do not produce high-energy neutrinos. The Earth's capture rate is derived from the Sun's capture rate using the Sun-to-Earth capture ratio given in Figure 1 of [63]. The curve is approximately $\gamma = \log_{10}(m_{\chi}^4) - 6.35$. This is consistent with the capture ratios calculated in the supersymmetric models (Figure 20). The relic density re-calculation is performed only on models with $m_{\chi} > 80$ GeV. Capture resonances in the Earth make the capture ratio very sensitive to m_{χ} below this range, and this is where κ has its largest variations. These uncertainties would most likely make a determination of $\Omega_{\chi} h^2$ in this range impossible.

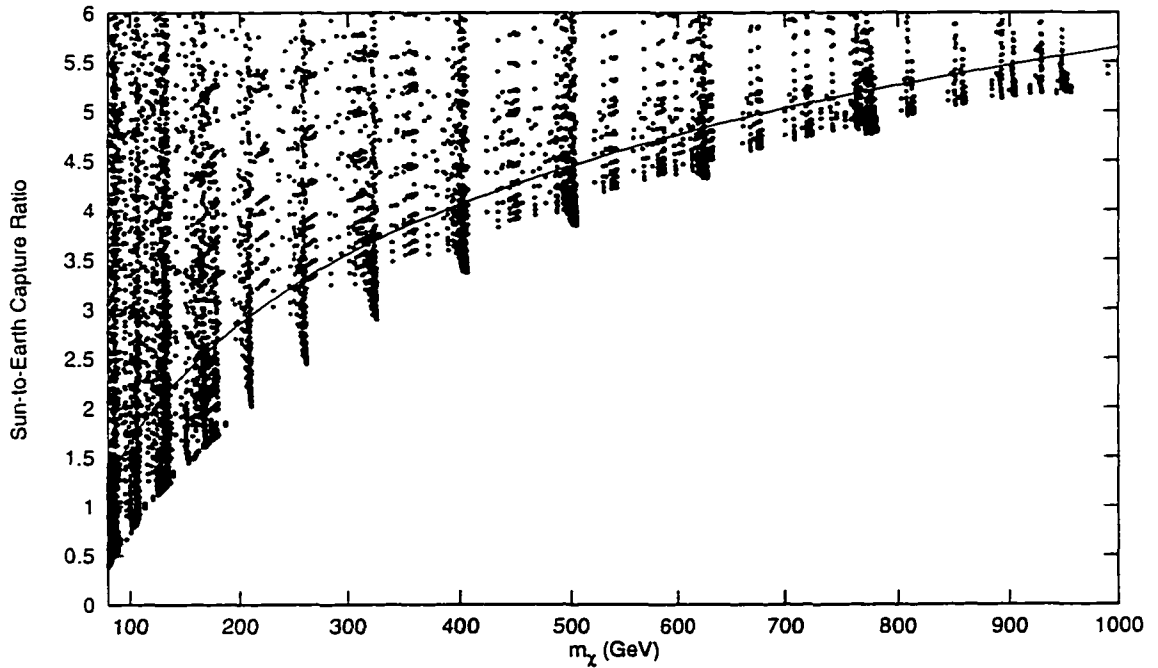


Figure 20: Sun-to-Earth capture ratio γ for a range of m_{χ} . The solid line is $\gamma = \log_{10}(m_{\chi}^4) - 6.35$. The range on the y-axis represents only the lower limit of γ ; points extend several orders of magnitude off the top of the figure for other models.

4.3.3 Scalar versus Axial-Vector Interactions

Finally, it is important to keep in mind that the relic density estimate is valid only if neutralinos are captured predominately through scalar (spin-independent) interactions. The presence of axial-vector (spin-dependent) interactions increases solar capture relative to the Earth, making it appear as if the Earth is either away from full signal when it is not, or further away from full signal than it actually is. For this reason, the density estimate is limited to scalar neutralinos only. The difficulty lies in knowing if the Earth's event rate is reduced because it is away from full signal, or because axial interactions dominate.

A comparison of direct and indirect event rates may provide some insight. The various kinds of direct detection experiments have different sensitivities to axial and scalar interactions. Typically, direct detectors are more sensitive to neutralinos with scalar couplings, while indirect detectors perform better for neutralinos with axial couplings. A comparison of event rates could yield information about neutralino couplings, as well as neutralino mass [27]. In general, it is clear that other sources of information about neutralinos would almost certainly be necessary to estimate their relic density in the universe.

5 Discussion and Conclusion

This work examines the muon event rate over a range of supersymmetric parameters that includes higher neutralino mass regimes (up to $\sim \text{TeV}$) not previously examined in a comprehensive way. These heavier masses become more important as areas of parameter space that produce mainly lighter neutralinos are gradually ruled out by experimental searches or other constraints. With large neutralino masses, decay channels not normally considered can become a factor in the event rate and are therefore included. An examination of the neutralinos arising from supersymmetric models provides an opportunity for investigating the ability to move from an event rate to gaining knowledge of neutralino properties should a detection occur. The calculation of muon event rates in a neutrino telescope has two main components: exploring the supersymmetric parameter space that creates good dark matter candidates, and modelling the production and propagation of high energy neutrinos from the annihilation of these candidate WIMPs in the Sun and Earth.

There are a few issues associated with the calculation of event rates that should be addressed. The first, alluded to earlier, is the question of assuming neutralinos make up the entire dark halo. This assumption is used throughout these calculations, except where the relic density is thought to be too small ($\Omega_\chi h^2 < 0.025$) to remain compatible with the local dark halo density. There is no strict theoretical or experimental basis for this assumption; it is simply the scenario chosen for examination here. Experimentally, MACHO searches have placed limits on certain mass ranges and distributions, but scenarios where MACHOs are the dominant component of local dark matter remain viable [18]. It is also somewhat disconcerting that such a wide range of relic densities ($0.025 < \Omega_\chi h^2 < 1$) is capable of producing the entire dark halo in models of galaxy formation. Nevertheless, the apparent lack of baryonic matter in the universe to account for dynamical observations, and the theoretical

arguments supporting a supersymmetric cold dark matter candidate such as the neutralino, make the halo density assumption a reasonable one. An indirect detection of high-energy neutrino events from neutralino annihilation would not constitute proof that neutralinos are *the* dark matter (galactic or universal), but it would be very strong circumstantial evidence.

Coannihilation, where a particle with a mass near that of the neutralino controls its annihilation in the early universe, is not included in the models. The process could suppress or increase the relic density, weakening the dependence on the neutralino annihilation cross section. This is a potential problem when doing a relic density estimate using the procedure outlined above, but it may not necessarily change event rates significantly. They depend more on the elastic scattering cross section and the local dark matter density than on the relic universal density. In certain regions of parameter space, the effects of coannihilation can be large and should be included [44, 37].

There are, of course, more exotic possibilities that might change the results presented here. Unusual early universe scenarios, such as a non-standard freezeout or expansion, could suppress or enhance the relic abundance of dark matter [66]. If the solar neutrino problem and anomalies in atmospheric neutrinos are caused by neutrino oscillations, the same process could alter the muon event rate in indirect detectors [40]. It is difficult to do more than note these possibilities here until further knowledge is gained about the neutralino or these scenarios.

The prospects for detecting supersymmetric dark matter in the near future are promising as new, more sensitive detectors come on-line. If an indirect detector does find evidence of neutralino annihilation in the Sun and Earth, the information contained in the event rates might provide information about the neutralino and the supersymmetric theory that underlies it. In particular, the ratio of events from the Sun and Earth is a useful quantity to consider. An event ratio that is much smaller

than one suggests the neutralino probably has a mass in the 50 – 60 GeV range, near the iron capture resonance.

The event ratio, in conjunction with knowledge about the neutralino's mass and annihilation characteristics, can also lead to limits on or an estimate of the relic density of neutralinos $\Omega_\chi h^2$. However, uncertainties involved with relating capture rates to event rates makes an accurate determination very difficult. In the future, as detector characteristics improve, information about the energy spectrum of high-energy neutrinos from neutralino annihilation may be available, allowing a reduction in the model dependent uncertainties [73]. Combining information collected from various detection schemes (accelerator, direct and indirect searches) to improve an estimate would be necessary. Uncertainties in modelling the galaxy and dark matter halos also need to be addressed. A 10% error in the local circular speed results in a 40% error in the local dark matter density [74]. Even if it is not possible to derive further information from an indirect detection beyond establishing the existence of supersymmetric particles, this in itself would be an important achievement with wide-ranging implications.

References

- [1] E. W. Kolb and M. S. Turner. *The Early Universe*. Frontiers In Physics. Allan M. Wyde. 1990 (and references therein).
- [2] A. M. Boesgaard and G. Steigman. Big bang nucleosynthesis: Theories and observations. *Annual Review of Astronomy and Astrophysics*, 23:319, 1985.
- [3] V. Trimble. Existence and nature of dark matter in the universe. *Annual Review of Astronomy and Astrophysics*, 25:425–472, 1987.
- [4] K. G. Begeman, A. H. Broeils, and R. H. Sanders. Extended rotation curves of spiral galaxies - dark haloes and modified dynamics. *Monthly Notices of the Royal Astronomical Society*, 249:523, 1991.
- [5] D. Zaritsky. The mass of spiral galaxy halos. *Publications of the Astronomical Society of the Pacific*, 104:831–834, September 1992.
- [6] R. P. Saglia et al. Stellar dynamical evidence for dark halos in elliptical galaxies: the case of NGC 4472, IC 4296, and NGC 7144. *The Astrophysical Journal*, 403:567–572, February 1993.
- [7] D. Fabricant and P. Gorenstein. Further evidence for M87's massive, dark halo. *The Astrophysical Journal*, 267:535–546, April 1983.
- [8] S. D. M. White et al. The baryon content of galaxy clusters - a challenge to cosmological orthodoxy. *Nature*, 366:429, December 1993.
- [9] A. Yahil, D. Walker, and M. Rowan-Robinson. The dipole anisotropies of the IRAS galaxies and the microwave background radiation. *The Astrophysical Journal*, 301L:1, February 1986.

- [10] Y. Sigad et al. IRAS versus POTENT density fields on large scales: Biasing parameter and Ω . *The Astrophysical Journal*, 495:516–532, March 1998.
- [11] M. R. S. Hawkins. Dark matter from quasar microlensing. *Mon. Not. R. Astron. Soc.*, 278:787–807, 1996.
- [12] A. H. Guth. *Physical Review D*, 23:347, 1981.
- [13] C. B. Collins and S. W. Hawking. Why is the universe isotropic? *The Astrophysical Journal*, 180:317–334, March 1973.
- [14] E. V. Stronach. A discussion of the flatness problem. Talk presented at *Beyond the Big Bang: Prospects and Challenges*, Kingston, December 1989.
- [15] C. Alcock et al. EROS and MACHO combined limits on planetary-mass dark matter in the galactic halo. *The Astrophysical Journal*, L499:9, May 1998.
- [16] C. Alcock et al. The MACHO project Large Magellanic Cloud microlensing results from the first two years and the nature of the galactic dark halo. *The Astrophysical Journal*, 486:697–726, September 1997.
- [17] B. Paczynski et al. The Optical Gravitational Lensing Experiment (OGLE). *Bulletin of the American Astronomical Society*, 187:14.07, December 1995.
- [18] E. I. Gates, G. Gyuk, and M. S. Turner. The local halo density. *The Astrophysical Journal*, 449:L123–126, August 1995.
- [19] E. F. Bunn and M. White. The 4 year COBE normalization and large-scale structure. *The Astrophysical Journal*, 480:6–21, May 1997.
- [20] B. Carr. Baryonic dark matter. *Annual Review of Astronomy and Astrophysics*, 32:531, 1994.

- [21] R. Malaney and G. Matthews. Probing the early universe: a review of primordial nucleosynthesis beyond the standard big bang. *Physics Reports*, 229:145–219, 1993.
- [22] S. L. Glashow. Partial-symmetries of weak interactions. *Nuclear Physics*, 22:579, 1961.
- [23] S. Weinberg. A model of leptons. *Physical Review Letters*, 19:1264, 1967.
- [24] A. Salam. *Elementary Particle Theory*, page 367. Almquist and Wiksells, Stockholm, 1969.
- [25] D. Politzer. Asymptotic freedom: an approach to strong interactions. *Physics Reports*, 14:129, 1974.
- [26] F. Wilczek. *Ann. Rev. Nucl. Part. Sci.*, 32:177, 1982.
- [27] G. Jungman, M. Kamionkowski, and K. Griest. Supersymmetric dark matter. *Physics Reports*, 267(5.6):195–373, March 1996.
- [28] M. F. Sohnius. Introducing supersymmetry. *Physics Reports*, 128(2.3):39–204, 1985.
- [29] P. Langacker. Grand unification and the standard model. Talk presented at *Radiative Corrections: Status and Outlook*, Gatlinburg, TN, June 1994.
- [30] S. Dimopoulos, S. A. Raby, and F. Wilczek. Proton decay in supersymmetric models. *Physics Letters B*, 112:133, 1982.
- [31] U. Amaldi, W. de Boer, and H. Fürstenan. Comparison of grand unified theories with electroweak and strong coupling constants measured at LEP. *Physics Letters B*, 260:447, May 1991.

- [32] S. Dawson. R-parity breaking in supersymmetric theories. *Nuclear Physics B*, 261:297–318, 1985.
- [33] T. Kobayashi, S. Kitamura, and T. Kon. Supersymmetric particle production at HERA. *International Journal of Modern Physics*, A11:1875–1912, 1996.
- [34] K. Griest, M. Kamionkowski, and M. S. Turner. Supersymmetric dark matter above the W mass. *Physical Review D*, 41:3565, 1990.
- [35] B. W. Lee and S. Weinberg. WIMP relic abundance. *Physical Review Letters*, 39:165, 1977.
- [36] K. Griest. The nature of the dark matter. In *Varenna 1995, Dark Matter in the universe*, October 1995. Preprint astro-ph/9510089.
- [37] J. Edsjö and P. Gondolo. Neutralino relic density including coannihilations. *Physical Review D*, 56:1879–1894, 1997.
- [38] K. Griest and D. Seckel. Cosmic asymmetry, neutrinos, and the Sun. *Nuclear Physics B*, 283:681, 1987.
- [39] G. R. Blumenthal, S. M. Faber, J. R. Primack, and M. J. Rees. Formation of galaxies and large-scale structure with cold dark matter. *Nature*, 311:517, 1984.
- [40] M. Mori et al. Search for neutralino dark matter heavier than the W boson at Kamiokande. *Physical Review D*, 48(12), December 1993.
- [41] J. M. LoSecco et al. Limits on the flux of energetic neutrinos from the Sun. *Physics Letters*, B188:388, 1987.
- [42] M. Mori et al. Search for neutralino dark matter in Kamiokande. *Physics Letters*, B270:89, 1991.

- [43] M. Mori et al. A limit on massive neutrino dark matter from Kamiokande. *Physics Letters*. B289:463, 1992.
- [44] J. Edsjö. *Aspects of neutrino detection of neutralino dark matter*. PhD thesis. Uppsala University. Department of Theoretical Physics, April 1997.
- [45] G. Jungman, K. Griest, and M. Kamionkowski. *Neutdriver Version 1.0*. June 1995.
- [46] R. M. Barnett et al. Review of particle physics. *Physical Review D*, 54(1), (1996) and 1997 off-year partial update for the 1998 edition (URL <http://pdg.lbl.gov/>).
- [47] B. Chaboyer et al. The age of globular clusters in light of Hipparcos: Resolving the age problem? *The Astrophysical Journal*, 494:96, February 1998.
- [48] J. L. Feng, N. Polonsky, and S. Thomas. The light higgsino-gaugino window. *Physics Letters B*, 370:95–105, 1996.
- [49] J. Faulkner. Remarks on the evolution of low-mass stars: More or less opaque? In *Challenges to Theories of the Structure of Moderate-Mass Stars*, 1991.
- [50] J. Faulkner and R. L. Gilliland. Weakly interacting, massive particles and the solar neutrino flux. *The Astrophysical Journal*, 299:994–1000, December 1985.
- [51] J. Faulkner, D. O. Gough, and M. N. Vahia. Weakly interacting massive particles and solar oscillations. *Nature*, 321:226–231, May 1986.
- [52] R. L. Gilliland and W. Däppen. Oscillations in solar models with weakly interacting massive particles. *The Astrophysical Journal*, 324:1153–1157, January 1988.
- [53] R. L. Gilliland et al. Solar models with transport by weakly interacting particles. *The Astrophysical Journal*, 306:703–709, July 1986.

- [54] D. N. Spergel and W. H. Press. Effect of hypothetical, weakly interacting, massive particles on energy transport in the solar interior. *The Astrophysical Journal*, 294:663–673, July 1985.
- [55] J. Christensen-Dalsgaard. Solar models with enhanced energy transport in the core. *The Astrophysical Journal*, 385:354–362, January 1992.
- [56] Elsworth et al. Evidence from solar seismology against non-standard solar-core models. *Nature*, 347:536–539, October 1990.
- [57] H. Saio. Opacity in the solar radiative interior inferred from 5-min oscillations. *Monthly Notices of the Royal Astronomical Society*, 258(3):491–496, 1992.
- [58] D. N. Spergel and J. Faulkner. Weakly interacting, massive particles in horizontal-branch stars. *The Astrophysical Journal*, 331:L21–L24, August 1988.
- [59] D. O. Caldwell et al. Laboratory limits on galactic cold dark matter. *Physical Review Letters*, 61:510–513, August 1988.
- [60] W. H. Press and D. N. Spergel. Capture by the Sun of a galactic population of weakly interacting massive particles. *The Astrophysical Journal*, 296:679–684, September 1985.
- [61] A. Gould. Resonant enhancements in weakly interacting massive particle capture by the Earth. *The Astrophysical Journal*, 321:571–585, October 1987.
- [62] A. Gould. Weakly interacting massive particle distribution in and evaporation from the Sun. *The Astrophysical Journal*, 321:560–570, October 1987.
- [63] A. Gould. Cosmological density of WIMPs from solar and terrestrial annihilations. *The Astrophysical Journal*, 388:338–344, May 1988.

- [64] A. Gould. Gravitational diffusion of solar system WIMPs. *The Astrophysical Journal*, 368:610–615, February 1991.
- [65] A. Gould. Direct and indirect capture of weakly interacting massive particles by the Earth. *The Astrophysical Journal*, 328:919–939, April 1992.
- [66] M. Kamionkowski. Energetic neutrinos from heavy-neutralino annihilation in the Sun. *Physical Review D*, 44(10):3021–3042, November 1991.
- [67] S. Ritz and D. Seckel. Detailed neutrino spectra from cold dark-matter annihilations in the Sun. *Nuclear Physics B*, 304:877–908, 1988.
- [68] G. Jungman and M. Kamionkowski. Neutrinos from particle decay in the Sun and Earth. *Physical Review D*, 51:328, 1995.
- [69] E. I. Gates, M. Kamionkowski, and M. S. Turner. Comment on “The dispersion velocity of galactic dark matter particles”. *Physical Review Letters*, 78:2261, 1997.
- [70] M. Kamionkowski, L. M. Krauss, and M. T. Ressell. Implications of recent nucleon spin structure measurements for neutralino dark matter detection. Preprint hep-ph/9402353. June 1994.
- [71] K. Griest. Cross-sections, relic abundance and detection rates for neutralino dark matter. *Physical Review D*, 38:2357, 1988.
- [72] J. Edsjö and P. Gondolo. Wimp mass determination with neutrino telescopes. *Physics Letters B*, 357:595–601, 1995.
- [73] L. Bergström, J. Edsjö, and M. Kamionkowski. Astrophysical-neutrino detection with angular and energy resolution. *Astroparticle Physics*, 7:147–160, 1997.

- [74] D. N. Spergel. Particle dark matter. To be published in *Some Outstanding Questions in Astrophysics*, ed. by J. J. N. Bahcall and P. Ostriker. Preprint astro-ph/9603026. March 1996.

Acknowledgements

This thesis would not have been possible without the guidance and assistance of my thesis advisor Malcolm Butler, who possessed seemingly boundless patience, even when this work was interrupted by a trip to the far side of the planet.

I am also indebted (literally and figuratively) to my parents Andre and Marcia, who have provided support throughout my academic career.

Curriculum Vitae

Stefan H. P. Elieff

EDUCATION

Master of Science in Astronomy
Saint Mary's University
Halifax, Nova Scotia
1994-1998

Bachelor of Science in Physics (Honours)
St. Francis Xavier University
Antigonish, Nova Scotia
1990-1994

EMPLOYMENT

National Science and Engineering Research Council
Summer Research Grant
Carleton University
Department of Physics
May-August 1994

Summer Research Assistant
National Research Council of Canada
Herzberg Institute of Astrophysics
Solar-Terrestrial Physics Section
May-August 1993

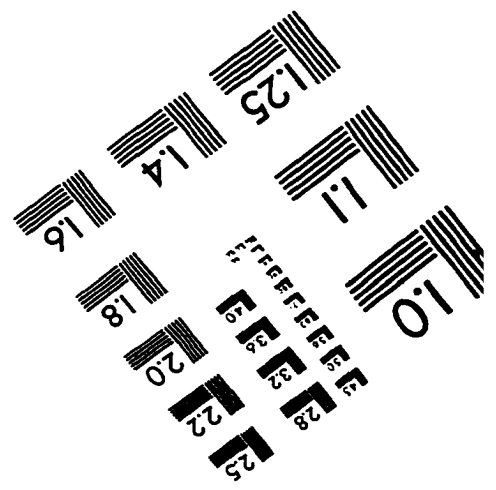
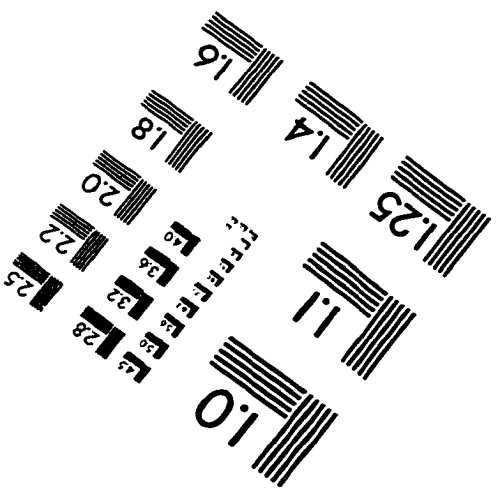
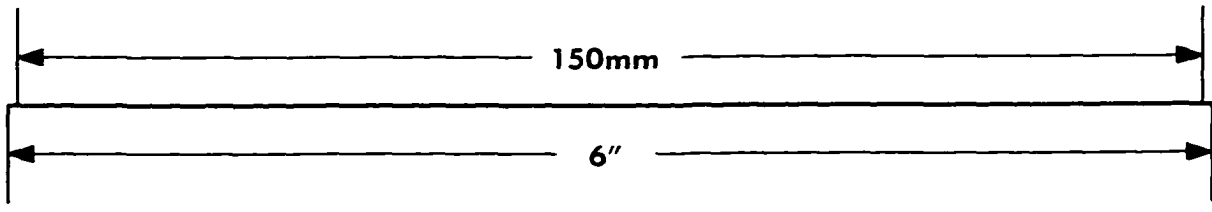
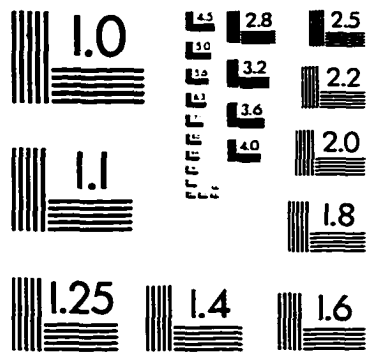
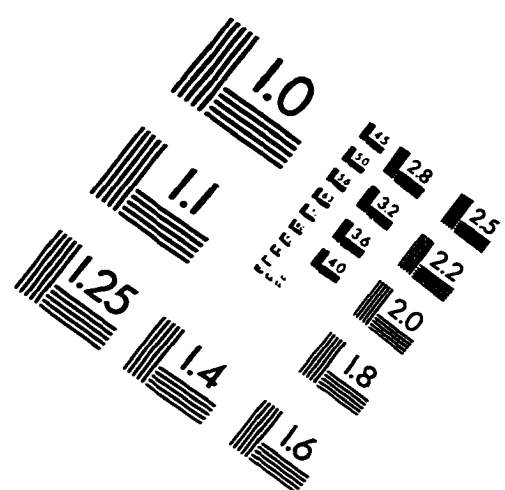
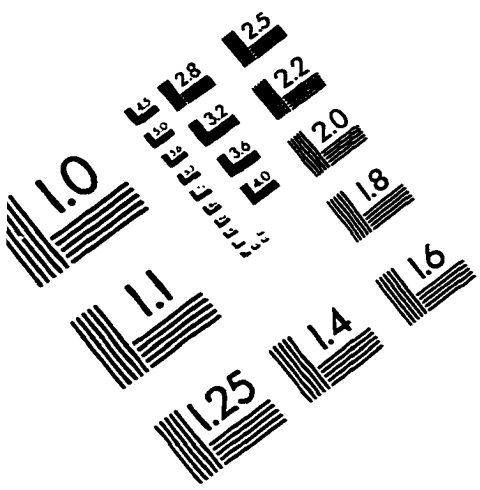
Summer Research Assistant
National Research Council of Canada
Herzberg Institute of Astrophysics
Solar-Terrestrial Physics Section
May-August 1992

Summer Research Assistant
National Research Council of Canada
Institute for Microstructural Sciences
May-August 1991

PUBLICATIONS

M. Blake, T. Fuller, D. J. Lane, J. Asbell-Clarke, S. Mitchell, S. Elieff. Supernova 1995F in NGC 2726. *IAU Circ.*, 6153, 3 (1995).

IMAGE EVALUATION TEST TARGET (QA-3)



APPLIED IMAGE, Inc
1653 East Main Street
Rochester, NY 14609 USA
Phone: 716/482-0300
Fax: 716/288-5989

© 1993, Applied Image, Inc., All Rights Reserved